ORIGINAL PAPER

Probabilistic SDDLV method for localizing damage in bridges monitored within one cluster under time-varying environmental temperatures

Jianxin Cao[1] · Shaoyi Zhang[1] · Yang Liu[1]

Abstract

The stochastic dynamic damage location vector (SDDLV) method has been widely utilized for localizing damage in structures. However, under changing environmental temperatures, its accuracy is greatly reduced, and the method may even lose efficacy. Furthermore, there has been no investigation of how SDDLV could localize damage in all bridges that are simultaneously monitored within one cluster, i.e., several medium- and small-span bridges with the same structural design on a continuous elevated corridor. To address these issues, a probabilistic SDDLV method is proposed in this study. First, unlike the conventional SDDLV method, the damage location vectors (DLVs) are generated using acceleration monitoring data acquired in the same period that are obtained from each pair of identical bridges among all the monitored bridges in one cluster. Second, considering variations in the finite element model (FEM) of bridges with respect to the environmental temperature, the probabilistic FEM is applied to replace the regular definite FEM, which is utilized to calculate the stresses of all the elements of the structures. Third, a method based on the probability characteristics of the damage localization index is presented to determine the thresholds of damage localization. Then, by incorporating hypothesis testing and a cross-validation strategy, the structural damage of all monitored bridges within one cluster is localized. Finally, a numerical simulation example is utilized to verify the effectiveness of the proposed method, and the effect of structural deviations in construction on the damage localization results is analyzed through the monitoring data of actual bridges.

Keywords Bridges monitored within one cluster · Damage localization of structures · Time-varying environmental temperature · Probabilistic finite element model · Cross-validation strategy

1 Introduction

Damage diagnosis methods for bridges have been widely studied as the core content of structural health monitoring in recent decades. Vibration-based damage diagnosis methods have the advantages of nondestructive detection and a high damage detection efficiency, and they have become the focus of attention [1–4]. However, damage localization for bridges is a challenging issue in the field of structural damage diagnosis. At present, damage localization methods are mainly classified into model-based methods and data-driven

methods. Model-based methods mainly update the physical parameters of the FEMs of bridges to minimize the discrepancy between the measured response and the analytical response, and the damage is localized to the elements in which the parameters are updated [5, 6]. For data-driven methods, the damaged regions of bridges are localized using changes to the damage features, such as the mode shapes and modal curvature [7], modal strain energy [8], frequency response function [9] and flexibility matrix [10]. Additionally, many data processing methods, which mainly include time-domain vibration signal processing [11], wavelet analysis [12], artificial neural networks [13], deep learning [14] and Bayesian theory [15], have also been applied in damage localization for bridges.

Among these methods, the DLV method is proposed to generate a vector by solving the null space of the flexibility matrix residual between the damaged and healthy structures [16]. When this vector is treated as a set of loads in the FEM

✉ Yang Liu
  ly7628@hit.edu.cn

1 School of Transportation Science and Engineering, Harbin Institute of Technology, 73 Huanghe Road, Harbin 150090, China

Ⓐ Springer

of the undamaged structure, the elements with zero stress are candidates for damage. Subsequently, the DLV method was extended, including the stochastic damage location vector (SDLV) method [17], the dynamic damage location vector (DDLV) method [18] and the SDDLV method [19]. Gao et al. used a laboratory-scale truss model to verify the effectiveness of the DLV method based on experimental data [20]. Additionally, the SDLV method has been applied to a full-scale historic truss bridge [21, 22]. The SDDLV method uses only the output responses of sparse sensors to localize the damage, and the transfer function matrix is utilized in this method to obtain more information about the structural damage.

The SDDLV method assumes that the environmental conditions are constant; however, a bridge is in a constantly changing environment throughout its life cycle. Variations in the environmental temperature will lead to changes in the material properties, joint stiffness and boundary conditions of the bridge, which usually obscure the actual damage to the bridge [23, 25]. The 1-year monitoring data on the Z24 Bridge revealed a 10% increase in the first two frequencies when the temperature decreased from 0 to − 7 °C [26]. Liu and DeWolf performed regression analysis on the 1-year modal data of a curved concrete box bridge, and the first three frequencies decreased by 0.5%, 0.7% and 0.3% per degree Celsius [27]. Farrar and Jauregui simulated beam damage by cutting the I-40 bridge from the web center to the bottom flange, resulting in decreases of 7.7%, 4.1% and 0.3% in the first three frequencies [28]. Therefore, the frequency variations in a bridge caused by such major damage are at the same level as those caused by variations in the environmental temperature.

Jang et al. used the SDLV method to localize the permanent tilt of a curved box girder bridge in Connecticut, USA [29]. However, this study used only acceleration data under several similar temperatures before and after damage to verify the SDLV method. Döhler et al. derived the uncertain boundary of damage localization results through the SDDLV method [30–32]. On this basis, the sensitivity of structural stiffness to temperature was used to update the modal parameters of the structure in the damaged state, and the damage region was determined by hypothesis testing [33]. However, it is difficult to choose the optimal installation location of temperature sensors for bridges [34, 35], and a large number of temperature sensors are usually required [36]. Furthermore, the accuracy of the sensitivity of the structural stiffness with respect to temperature cannot be guaranteed. To date, the SDDLV method has not been effectively applied to real-time damage localization for bridge structures under time-varying environmental temperatures.

In addition, some methods have been proposed to eliminate the effect of the environmental temperature in other studies on damage detection in bridges [25, 37–41]. Wang et al. localized cable damage by establishing a correlation model between the displacement of the main girder, the cable force and the environmental temperature [42]. Fallahian et al. proposed a damage detection method combining sparse coupled coding and a deep neural network, which effectively localized the damage of the I-40 bridge under time-varying temperature conditions [43]. Wang et al. proposed a damage detection method based on the covariance matrix of the acceleration response. The effect of the temperature variations on the diagonal elements of the matrix was reduced using a support vector machine, and then simulated damage to a suspension bridge was successfully detected [44]. Zhang et al. extracted damage features based on a time series analysis under time-varying temperatures, and the damage features were applied to an auto-associated neural network to eliminate the effect of the environmental temperature on damage localization for bridges [45]. However, these methods mainly focused on damage detection for a single bridge with environmental temperature variation, and little research has concentrated on damage localization for several bridges that are monitored in a cluster by utilizing the characteristics of similar environmental conditions.

The bridges monitored within one cluster are a set of several bridges with the same structural design on a continuous elevated corridor, and the mileage of such bridges is usually several kilometers. They are subject to similar traffic and environmental loads. In China, bridges monitored within one cluster are common, e.g., continuous urban viaducts, continuous highway bridges and high-speed railway bridges, as shown in Fig. 1. The similarity of the traffic loads implies that all the bridges monitored within one cluster have a similar level of traffic or even the same traffic in a certain region; hence, an annual increase in traffic volume will have a similar or identical impact on all bridges monitored in one cluster. The similarity of the environmental load implies that the environmental temperature around the bridges, the sunshine time and the wind load are similar. The authors previously proposed two damage diagnosis methods for bridges monitored within one cluster under time-varying temperatures [46, 47]. These methods can mitigate the effect of the environmental temperature; however, they cannot localize the damage. In this study, a probabilistic SDDLV method is proposed for damage localization in bridges monitored within one cluster under time-varying environmental temperatures. For the proposed method, the following aspects are different from those of the SDDLV method. First, with the probabilistic SDDLV method, the DLVs are generated using acceleration monitoring data acquired in the same period that are obtained from two identical bridges among all the bridges monitored within one cluster. Second, the regular definite FEM, utilized to calculate the stresses of all the elements of the structures, is replaced by the probabilistic FEM, which represents the variations in the FEM of the bridge under
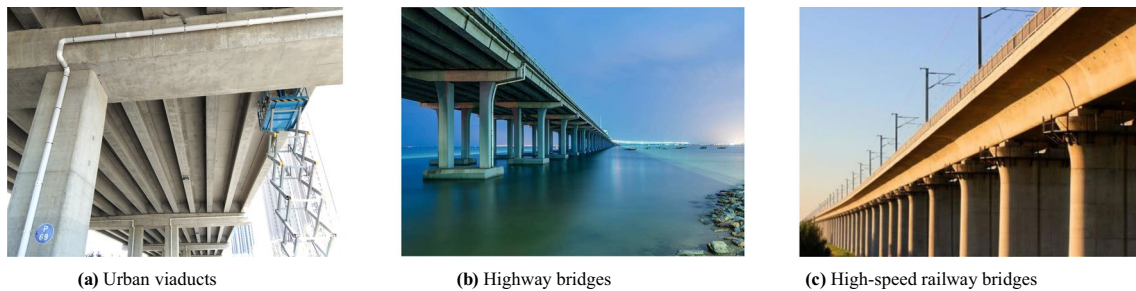
(a) Urban viaducts   **(b)** Highway bridges   **(c)** High-speed railway bridges

Fig. 1 The bridges monitored within one cluster

different environmental temperatures. Third, the thresholds of damage localization are determined by considering the probability characteristics of the damage localization index, and then a cross-validation strategy combined with a hypothesis test is presented to localize the damage of all monitored bridges. With the abovementioned characteristics of probabilistic SDDLV, the effect of temperature variations is effectively reduced, and the structural damage of all the bridges monitored within one cluster is localized.

2 The limitations of the SDDLV method under time-varying environmental temperatures

The SDDLV method is a damage localization method that uses the output-only vibration response and structural FEM [19]. In this method, the DLV is obtained by solving the null space of the residual of the transfer function matrix between the damaged and healthy structures. Then, the DLV is treated as a set of loads in the FEM for the computation of a stress field over the structure. The damage is localized at the points where the computed stress is zero or close to zero in practice [19, 32].

For a bridge structure, the equations of motion are shown in Eqs. (1) and (2) under healthy and damaged states, respectively.

$$\mathbf{M}\ddot{\boldsymbol{\eta}}_{\mathrm{h}}(t) + \mathbf{C}\dot{\boldsymbol{\eta}}_{\mathrm{h}}(t) + \mathbf{K}\boldsymbol{\eta}_{\mathrm{h}}(t) = \mathbf{F}_{\mathrm{h}}(t), \tag{1}$$

$$\mathbf{M}\ddot{\boldsymbol{\eta}}_{\mathrm{d}}(t) + \mathbf{C}\dot{\boldsymbol{\eta}}_{\mathrm{d}}(t) + (\mathbf{K} + \Delta\mathbf{K})\boldsymbol{\eta}_{\mathrm{d}}(t) = \mathbf{F}_{\mathrm{d}}(t), \tag{2}$$

where $\mathbf{M}, \mathbf{C}, \mathbf{K} \in \mathbb{R}^{n \times n}$ denote the mass, damping and stiffness matrix of the bridge, respectively; the subscripts h and d denote the healthy and damaged states, respectively; n denotes the total number of degrees of freedom (DOFs) of the bridge; $\boldsymbol{\eta} \in \mathbb{R}^{n \times 1}$ collects the displacements of the n DOFs; and $\mathbf{F} \in \mathbb{R}^{n \times 1}$ is the external load. As Eq. (2) shows, the structural damage is caused by the attenuation of stiffness. If requirements are imposed such that the external

loads $\mathbf{F}_{\mathrm{h}}(t)$ and $\mathbf{F}_{\mathrm{d}}(t)$ are the same and the displacement vectors $\boldsymbol{\eta}_{\mathrm{h}}(t)$ and $\boldsymbol{\eta}_{\mathrm{d}}(t)$ are equal under the healthy and damaged states, the following equation can be obtained by subtracting Eq. (2) from Eq. (1).

$$\Delta\mathbf{K}\hat{\boldsymbol{\eta}}(t) = 0, \tag{3}$$

where $\hat{\boldsymbol{\eta}}(t)$ denotes the displacement vectors under the healthy and damaged states. Equation (3) shows that loads that lead to identical responses in both states exist when the change in the stiffness matrix is rank deficient.

When the DLV is treated as a set of loads in the FEM, the structural strain energy under the healthy state and damaged state can be expressed as

$$\mathbf{U}_{\mathrm{h}} = \frac{1}{2}\hat{\boldsymbol{\eta}}^{\mathrm{T}}\mathbf{K}\hat{\boldsymbol{\eta}} = \frac{1}{2}\left(\sum_{\Omega_{\mathrm{U}}} \hat{\mathbf{e}}_{a}^{\mathrm{T}}\mathbf{k}_{\mathrm{h},a}\hat{\mathbf{e}}_{a} + \sum_{\Omega_{\mathrm{D}}} \hat{\mathbf{e}}_{b}^{\mathrm{T}}\mathbf{k}_{\mathrm{h},b}\hat{\mathbf{e}}_{b}\right), \tag{4}$$

$$\mathbf{U}_{\mathrm{d}} = \frac{1}{2}\hat{\boldsymbol{\eta}}^{\mathrm{T}}(\mathbf{K} + \Delta\mathbf{K})\hat{\boldsymbol{\eta}} = \frac{1}{2}\left(\sum_{\Omega_{\mathrm{U}}} \hat{\mathbf{e}}_{a}^{\mathrm{T}}\mathbf{k}_{\mathrm{h},a}\hat{\mathbf{e}}_{a} + \sum_{\Omega_{\mathrm{D}}} \hat{\mathbf{e}}_{b}^{\mathrm{T}}(\mathbf{k}_{\mathrm{h},b} + \Delta\mathbf{k}_{b})\hat{\mathbf{e}}_{b}\right), \tag{5}$$

where $\hat{\mathbf{e}}_{a}$ and $\hat{\mathbf{e}}_{b}$ denote the node displacement vectors of elements a and b, which are portions of vector $\hat{\boldsymbol{\eta}}$; $\mathbf{k}_{\mathrm{h}}$ and $\mathbf{k}_{\mathrm{d}}$ denote the healthy and damaged element stiffness matrices, respectively; and Ω_{U} and Ω_{D} refer to the healthy and damaged parts of the domain. When damage occurs, assuming that the mass matrix $\mathbf{M}$ and damping matrix $\mathbf{C}$ are unchanged by the damage, the kinetic energy dissipated by damping and the work of the applied loading have identical histories in the healthy and damaged states. Therefore, according to the energy balance, the strain energy histories $\mathbf{U}_{\mathrm{h}}$ and $\mathbf{U}_{\mathrm{d}}$ must also be the same, and the following equation can be obtained by subtracting Eq. (5) from Eq. (4).

$$\sum_{\Omega_{\mathrm{D}}} \hat{\mathbf{e}}_{b}^{\mathrm{T}}\Delta\mathbf{k}_{b}\hat{\mathbf{e}}_{b} = 0. \tag{6}$$

Since Eq. (6) has a quadratic form, $\Delta\mathbf{k}_{b}$ is negative semidefinite, and $\hat{\mathbf{e}}_{b}$ is the rigid body motion. It can be concluded that Eq. (6) is satisfied only if each term of it is zero.

Therefore, when the DLV is treated as a set of loads in the FEM of the healthy structure, an element with zero stress is a candidate for damage.

The proof procedure of the SDDLV method shows that this method does not consider the effect of the environmental temperature on the damage localization results. Therefore, in Eqs. (4) and (5), the strain energy of the undamaged region before and after the occurrence of damage will no longer be equal; namely,

$$\sum_{\Omega_U} \hat{\mathbf{e}}_a^T \mathbf{k}_{h,a}(T_1) \hat{\mathbf{e}}_a \neq \sum_{\Omega_U} \hat{\mathbf{e}}_a^T \mathbf{k}_{h,a}(T_2) \hat{\mathbf{e}}_a, \tag{7}$$

where $\mathbf{k}_{h,a}(T_1)$ and $\mathbf{k}_{h,a}(T_2)$ denote the structural element stiffness matrices at temperatures T_1 and T_2, respectively. If there is a large difference in the environmental conditions in the healthy and damaged states, the precision of the DLV will be greatly reduced, even if the DLV is no longer applicable. Therefore, when the SDDLV method is used to localize the structural damage of bridges, it is necessary to consider the effect of environmental temperature variations.

3 Generation of the DLV based on the structural characteristics of bridges monitored within one cluster

In China, among bridges that are monitored within one cluster, there are often multiple bridges with the same structural design and construction time, such as urban viaducts, highway bridges and high-speed railway bridges, on a continuous elevated corridor. These bridges are subject to similar traffic and environmental loads in the same monitoring period. A schematic diagram of bridges monitored in a cluster is shown in Fig. 2, but it is not limited to continuous bridges.

To overcome the limitations of the SDDLV method under time-varying environmental temperatures, a method is proposed to generate DLVs using the structural acceleration response acquired in the same period from any two identical bridges, based on the idea that the structural designs are identical and the environmental temperatures are similar for the bridges monitored within one cluster. Utilizing the acceleration data, the transfer function matrix of each bridge is

determined, and the residual between the transfer function matrices of any two bridges in the same monitoring period is established, as shown in Eq. (8).

$$\Delta \mathbf{G} = \mathbf{G}_i(T) - \mathbf{G}_j(T) = \left[\mathbf{M}_i s^2 + \mathbf{C}_i s + \mathbf{K}_i(T)\right]^{-1} - \left[\mathbf{M}_j s^2 + \mathbf{C}_j s + \mathbf{K}_j(T)\right]^{-1} \tag{8}$$

where $\Delta \mathbf{G}$ is the residual between the transfer function matrices of any two bridges; $\mathbf{G}$ is the transfer function matrix of the bridge in any monitoring period; the subscripts i and j denote the number of bridges; and s is the Laplace variable.

Equation (8) shows that the stiffness matrix $\mathbf{K}(T)$ of bridges is a function of the temperature T. When bridges i and j are healthy, the values of $\mathbf{K}_i(T)$ and $\mathbf{K}_j(T)$ are equal in the same monitoring period. Therefore, the residual between the transfer function matrix of any two bridges does not change with temperature variations. Assuming that damage only causes attenuation of the structural stiffness, when damage occurs in one of the bridges, $\mathbf{K}_i(T)$ and $\mathbf{K}_j(T)$ will no longer be equal. At this time, the residual of the transfer function matrix is affected not only by measurement noise and identification errors in the modal parameters but also by the variation in the environmental temperature, as shown in Eq. (9).
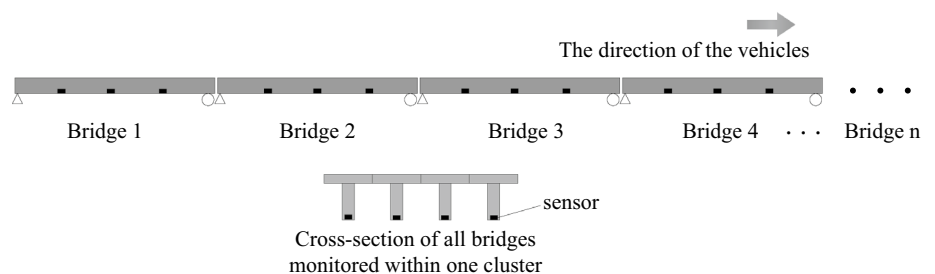
$$\begin{cases} \Delta \mathbf{G} = \mathbf{G}_i(T) - \mathbf{G}_j(T) = \delta \text{ The bridge structures are healthy} \\ \Delta \mathbf{G} = \mathbf{G}_i(T) - \mathbf{G}_j(T) = \Delta \mathbf{G}_d(T) + \delta \text{ The bridge structures are damaged} \end{cases}, \tag{9}$$

where δ denotes the calculated errors due to measurement noise and modal truncation; $\Delta \mathbf{G}_d(T)$ denotes the residual of the transfer function matrix when one of the bridges is damaged, which is affected by temperature variations.

Since the external load of the bridge is unknown, the transfer function matrix of the bridges cannot be generated directly using the monitoring acceleration data. The null space of $\Delta \mathbf{G}$ under each monitoring period can be obtained by solving the null space of $\Delta \mathbf{R}^T$ based on singular value decomposition, as derived in detail in [19],

$$\left[\mathbf{R}_i(T) - \mathbf{R}_j(T)\right]^T = \left[\mathbf{U}_1 \ \mathbf{U}_2\right] \begin{bmatrix} \mathbf{E}_1 & \mathbf{0} \\ \mathbf{0} & \mathbf{E}_2 \end{bmatrix} \left[\mathbf{V}_1 \ \mathbf{V}_2\right]^H, \tag{10}$$

Fig. 2 Schematic diagram of bridges monitored in a cluster

The direction of the vehicles

Bridge 1   Bridge 2   Bridge 3   Bridge 4   · · · Bridge n

sensor

Cross-section of all bridges monitored within one cluster

where E_2 is a singular value matrix, the diagonal terms of which are approximately equal to 0, $E_2 \in \mathbb{R}^{z_0 \times z_0}$, and z_0 is the number of zero singular values. The superscript H denotes the conjugate transpose. $\mathbf{V}_2$ is the eigenvector corresponding to E_2. The damage localization vector $\boldsymbol{\nu}$ is a linear combination of any basis vectors in the null space $\mathbf{V}_2$, and generally, the last column of $\mathbf{V}_2$, corresponding to the smallest singular value, is selected. $\mathbf{R}$ in Eq. (10) is expressed as [19]:

$$\mathbf{R}(T) = -\mathbf{C}_c \left[\mathbf{A}_c(T)\right]^{-2} \left[s\mathbf{I} - \mathbf{A}_c(T)\right]^{-1} \left\{ \begin{array}{c} \mathbf{C}_c \left[\mathbf{A}_c(T)\right]^{-1} \\ \mathbf{C}_c \left[\mathbf{A}_c(T)\right]^{-2} \end{array} \right\}^{\dagger} \left[\begin{array}{c} \mathbf{I} \\ \mathbf{0} \end{array} \right],$$

(11)

where $\mathbf{I}$ denotes the identity matrix; $\mathbf{A}_c$ is the system matrix; and $\mathbf{C}_c$ is the output matrix, both of which can be obtained from the output-only vibration acceleration response. The superscript † denotes the Moore–Penrose pseudoinverse.

When the bridge structure is in the healthy state, the theoretical value of each element in the matrix $\Delta\mathbf{R}^T$ is 0. Therefore, the damage localization vector $\boldsymbol{\nu}$ in each monitoring period does not change with temperature variations. All the vectors $\boldsymbol{\nu}$ generated in each monitoring period are combined into the sample set shown in Eq. (12).

$$\boldsymbol{\nu} = \left[\boldsymbol{\nu}_1, \boldsymbol{\nu}_2, \cdots, \boldsymbol{\nu}_e, \cdots, \boldsymbol{\nu}_{e_h}\right]^T,$$

(12)

where $\boldsymbol{\nu}_e$ is the damage localization vector at the eth sampling time, $e \in \left(1, 2, \cdots, e_h\right)$, and e_h denotes the total number of samples of the damage localization vector in the healthy state. To localize the damage in all regions of the bridge with sparse sensors, the damage localization vector $\boldsymbol{\nu}_e$ needs to be expanded to a load vector on all DOFs of the FEM. The entries of the load vector corresponding to the sensor positions are those of $\boldsymbol{\nu}$, with zeros elsewhere. The expanded damage localization vector $\boldsymbol{\nu}_e \in \mathbb{R}^{1 \times n}$ is expressed as:

$$\boldsymbol{\nu}_e = \left\{ v_e^1, v_e^2, \cdots, v_e^{n_0}, \cdots, v_e^n \right\},$$

(13)

where n denotes the dimension of the damage localization vector after expansion, which is equal to the total number of DOFs of the FEM. On this basis, the sample mean and variance of any entry $v_e^{n_0}$ are defined as shown in Eqs. (14) and (15).

$$\mathrm{E}\left(v_e^{n_0}\right) = \frac{1}{e_h} \sum_{e=1}^{e_h} v_e^{n_0},$$

(14)

$$\mathrm{D}\left(v_e^{n_0}\right) = \frac{1}{e_h - 1} \sum_{e=1}^{e_h} \left[v_e^{n_0} - \mathrm{E}\left(v_e^{n_0}\right)\right]^2$$

(15)

Where $\mathrm{D}(\cdot)$ denotes the variance of the variable and $\mathrm{E}(\cdot)$ represents the mean of the variable. In the healthy state, since the damage localization vector does not change with temperature variations, when the total number e_h of samples

is large enough, both the estimated values of the mean and variance calculated in the above equation can be regarded as the mean and variance of the population $v_e^{n_0}$.

As discussed in the above analysis, if a bridge is damaged, the damage localization vector $\boldsymbol{\nu}$ will still be affected by the temperature variations for the state inquiring damage, so it should be treated as a set of loads acting on the bridge under different environmental temperatures. However, in practical applications, it is difficult to generate the FEM with respect to different environmental temperatures due to the large number of calculations required. Therefore, the probabilistic FEM, namely, the probability distribution of all the FEM samples under different environmental temperatures, is applied to replace the usual definite FEM, and it is utilized to calculate the stresses of all the elements of the structures for SDDLV in this study. To further reduce the effect of the temperature, the monitoring data of the temperature and natural frequency are classified into several clusters, and the frequencies that are relatively constant under the effect of temperature are sorted into a cluster. Then, the damage localization vectors under all monitoring periods are also classified based on the clustering results of the environmental temperature. The flowchart of damage localization for any two identical bridges monitored in one cluster is shown in Fig. 3.

4 The probabilistic SDDLV method of damage localization for bridges monitored within one cluster

4.1 Classification of DLVs and establishment of probabilistic FEMs

Assuming that m modes of natural frequencies are observed for a bridge, a matrix of natural frequency monitoring data is generated as

$$\mathbf{f} = \begin{bmatrix} f_{1,1} & f_{1,2} & \cdots & f_{1,m} \\ f_{2,1} & f_{2,2} & \cdots & f_{2,m} \\ \vdots & \vdots & \ddots & \vdots \\ f_{k,1} & f_{k,2} & \cdots & f_{k,m} \end{bmatrix},$$

(16)

where k is the number of natural frequency samples. Furthermore, the environmental temperature monitoring data are denoted as $\mathbf{T}$, and $\mathbf{T} \in \mathbb{R}^{k \times 1}$ is defined as

$$\mathbf{T} = \left\{ T_1, \ T_2, \ \ldots, \ T_k \right\}^T.$$

(17)

After obtaining $\mathbf{f}$ and $\mathbf{T}$, the data sample matrix $\boldsymbol{\Phi} \in \mathbb{R}^{k \times (m+1)}$ is defined as:

$$\boldsymbol{\Phi} = [\mathbf{T}, \mathbf{f}].$$

(18)

Using the Gaussian mixture model (GMM) cluster analysis method [48], the natural frequency and temperature
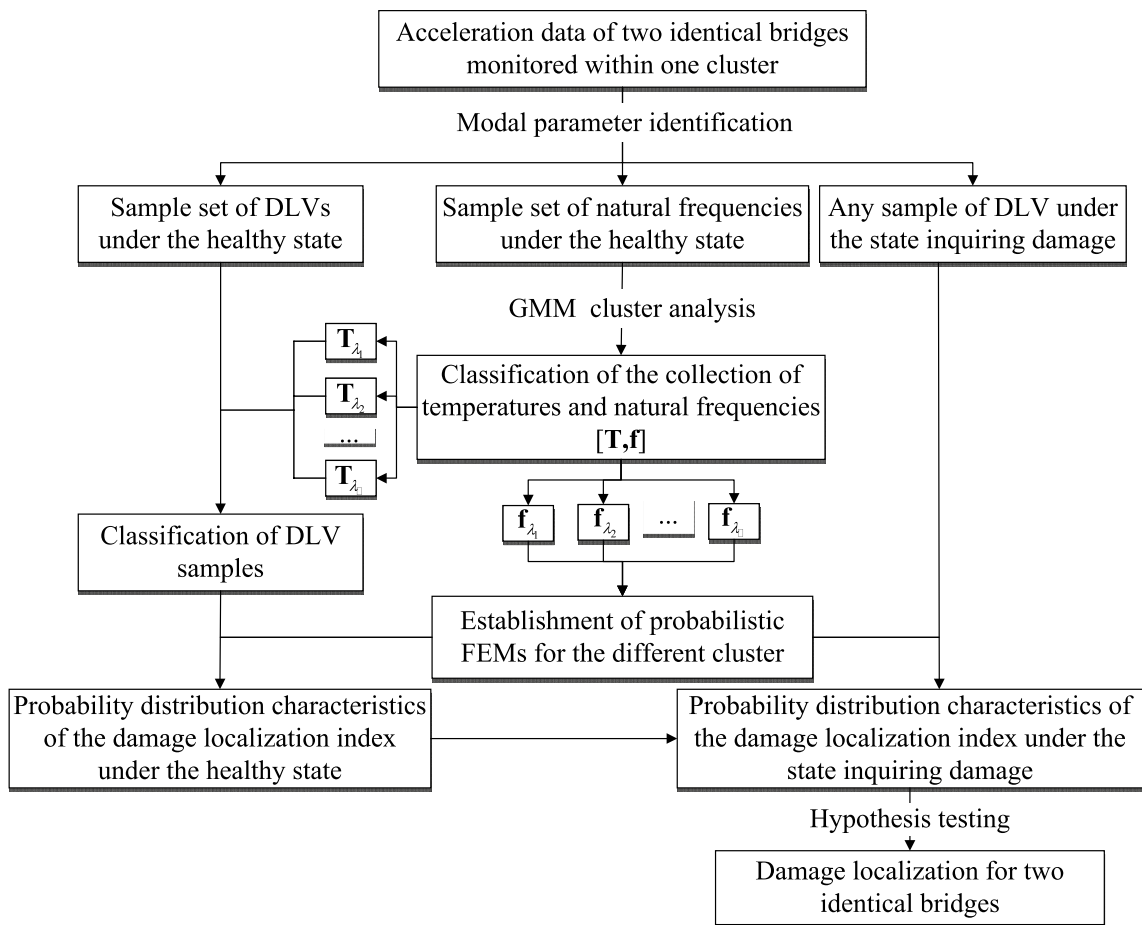
Fig. 3 Flowchart of damage localization for any two identical bridges monitored in a cluster

monitoring data of bridges under each monitoring period are classified into several clusters, and for each cluster, the sample of natural frequencies satisfies a Gaussian probability distribution, reflecting a similar environmental effect on the structural stiffness. The details of cluster analysis are described in the Appendix I. Using the temperature data after clustering as a pointer, the damage localization vectors obtained by Eq. (10) in each monitoring period are classified. The classification of the DLVs in any cluster λ is as follows:

$$\Gamma_\lambda = \left[\mathbf{T}_\lambda, \boldsymbol{\nu}_\lambda\right], \tag{19}$$

where the mean and variance of all terms in the damage localization vector $\boldsymbol{\nu}_\lambda$ is calculated according to Eqs. (14) and (15).

During the operation of an actual bridge, the global structural stiffness of the bridge changes with the variation in the environmental temperature. In this study, the probabilistic FEM under each cluster is established using the probabilistic FEM updating method [6]. In each cluster, the natural

frequency sample set is used as the updating target, and the temperature-related structural parameters, i.e., the structural material properties, node connection stiffness, boundary conditions, etc., are updated as random variables satisfying a certain probability distribution.

The set of sample estimation matrices $\tilde{\boldsymbol{\theta}}$ of the update parameters are expressed as:

$$\tilde{\boldsymbol{\theta}} = \left[\tilde{\boldsymbol{\theta}}_1, \tilde{\boldsymbol{\theta}}_2, \ldots, \tilde{\boldsymbol{\theta}}_k, \cdots, \tilde{\boldsymbol{\theta}}_r\right]_{r\times\upsilon}^{\mathrm{T}}, \tag{20}$$

where υ and r are the numbers of update parameters and total samples, respectively. Each term of this set is denoted as $\tilde{\boldsymbol{\theta}}_k$, where the superscript tilde represents its random characteristics. $\tilde{\boldsymbol{\theta}}_k$ is generated randomly by the Monte Carlo method, and it is defined as:

$$\tilde{\boldsymbol{\theta}}_k = \left\{\tilde{\theta}_{k,1}, \tilde{\theta}_{k,2}, \ldots, \tilde{\theta}_{k,\upsilon}\right\}. \tag{21}$$

On this basis, using the mean $\mathbf{E}\left(\mathbf{f}_\lambda\right)$ and covariance $\mathbf{Cov}\left(\mathbf{f}_\lambda\right)$ of the measured natural frequency data $\mathbf{f}_\lambda$ under each cluster, the mean and covariance of the update parameters

are undated based on the probability FEM updating method for bridges proposed in [6]. Then, the mean $\mathbf{E}(\tilde{\boldsymbol{\theta}}_\lambda)$ and covariance $\mathbf{Cov}(\tilde{\boldsymbol{\theta}}_\lambda)$ of the update parameters in any cluster λ are obtained. The mean and variance of each element in the transfer function matrix $\mathbf{G}_m(\tilde{\boldsymbol{\theta}})$ and element stiffness matrix $\mathbf{k}_m(\tilde{\boldsymbol{\theta}})$ of the FEM can be calculated as shown in the Appendix II. Thus, the probabilistic FEM of a bridge in any cluster is obtained and used to replace the regular definite FEMs under different temperatures.

4.2 Damage localization of two identical bridges monitored within one cluster

4.2.1 Calculation of the probability characteristics of the damage localization index in the healthy state

As discussed in the above section, the DLV is treated as a set of loads acting at the bridge to calculate the stress field, and a region with zero stress is a damage location. To obtain the structural stress field of the bridge in each monitoring period, first, any one of the bridges monitored within one cluster is selected as the reference bridge; this is different from the conventional method. On this basis, in the healthy state, the DLV generated using the monitoring data from the reference bridge and any other bridge is applied to the probabilistic FEM of the reference bridge. Then, the displacements at all DOFs are calculated as shown in Eq. (22).

$$\tilde{\boldsymbol{\zeta}}_{w,\mathrm{h}} = \mathbf{k}_{\mathrm{m},w}(\tilde{\boldsymbol{\theta}})\tilde{\mathbf{y}}_{w,\mathrm{h}}, \tag{23}$$

where $\tilde{\mathbf{y}}_{w,\mathrm{h}}$ is the nodal displacement vector of element w in the healthy state and $\mathbf{k}_{\mathrm{m},w}(\tilde{\boldsymbol{\theta}})$ is the element stiffness matrix of any element w of the probabilistic FEM of any cluster. Assuming that any element of the FEM contains φ DOFs, $\tilde{\boldsymbol{\zeta}}_{w,\mathrm{h}}$ is expressed as follows:

$$\tilde{\boldsymbol{\zeta}}_{w,\mathrm{h}} = \left\{ \tilde{\zeta}_{w,\mathrm{h}}^1, \ \tilde{\zeta}_{w,\mathrm{h}}^2, \ \cdots, \ \tilde{\zeta}_{w,\mathrm{h}}^{\varphi_0}, \ \cdots, \ \tilde{\zeta}_{w,\mathrm{h}}^{\varphi} \right\}^{\mathrm{T}}, \tag{24}$$

where $\tilde{\zeta}_{w,\mathrm{h}}^{\varphi_0}$ is the stress value corresponding to the φ_0th DOF of any element w, $\varphi_0 \in (1, 2, \cdots, \varphi)$. The damage localization index of any element w in the healthy state is defined as follows:

$$\tilde{\psi}_{w,\mathrm{h}} = \sum_{\varphi_0=1}^{\varphi} \tilde{\zeta}_{w,\mathrm{h}}^{\varphi_0}. \tag{25}$$

In the above calculation procedure, since the DLV contains errors of both modal parameter identification and measured noise and the probabilistic FEM of the bridge is random, it is necessary to calculate the variance of the damage localization index.

In Sect. 4.1, the mean and variance of each term in the DLV are calculated during all monitoring periods in the healthy state. Additionally, the mean and variance of each term in the transfer function matrix $\tilde{\mathbf{G}}_m$ of the probabilistic FEM is calculated in Sect. 4.2. On this basis, the variance of any node displacement $\tilde{y}_{\mathrm{h}}^{n_1}$ is derived as follows:

$$
\begin{aligned}
\mathrm{D}(\tilde{y}_{\mathrm{h}}^{n_1}) &= \mathrm{D}\left(\sum_{n_0=1}^{n} \tilde{G}_{\mathrm{m}}^{n_1,n_0} v_{\mathrm{h}}^{n_0} \right) = \sum_{n_0=1}^{n} \mathrm{D}(\tilde{G}_{\mathrm{m}}^{n_1,n_0} v_{\mathrm{h}}^{n_0}) \\
&= \sum_{n_0=1}^{n} \left\{ \mathrm{E}\left[(\tilde{G}_{\mathrm{m}}^{n_1,n_0})^2 (v_{\mathrm{h}}^{n_0})^2 \right] - \mathrm{E}(\tilde{G}_{\mathrm{m}}^{n_1,n_0} v_{\mathrm{h}}^{n_0})^2 \right\} \\
&= \sum_{n_0=1}^{n} \left\{ \mathrm{E}\left[(\tilde{G}_{\mathrm{m}}^{n_1,n_0})^2 \right] \mathrm{E}\left[(v_{\mathrm{h}}^{n_0})^2 \right] - \mathrm{E}(\tilde{G}_{\mathrm{m}}^{n_1,n_0})^2 \mathrm{E}(v_{\mathrm{h}}^{n_0})^2 \right\} \\
&= \sum_{n_0=1}^{n} \left\{ \left[\mathrm{D}(\tilde{G}_{\mathrm{m}}^{n_1,n_0}) + \mathrm{E}(\tilde{G}_{\mathrm{m}}^{n_1,n_0})^2 \right] \left[\mathrm{D}(v_{\mathrm{h}}^{n_0}) + \mathrm{E}(v_{\mathrm{h}}^{n_0})^2 \right] - \mathrm{E}(\tilde{G}_{\mathrm{m}}^{n_1,n_0})^2 \mathrm{E}(v_{\mathrm{h}}^{n_0})^2 \right\},
\end{aligned}
\tag{26}
$$

$$\tilde{\mathbf{y}}_{\mathrm{h}} = \mathbf{G}_{\mathrm{m}}(\tilde{\boldsymbol{\theta}})\boldsymbol{\nu}_{\mathrm{h}}, \tag{22}$$

where $\boldsymbol{\nu}_{\mathrm{h}}$ is the DLV of any cluster, and the subscript h denotes the healthy state; $\mathbf{G}_{\mathrm{m}}(\tilde{\boldsymbol{\theta}}) \in \mathbb{R}^{n \times n}$ is the transfer function matrix of the probabilistic FEMs of any cluster; $\tilde{\mathbf{y}}_{\mathrm{h}}$ is the nodal displacement vector of the bridge in a healthy state, and each term is also a random variable satisfying a certain probability distribution. Finally, the stress field $\tilde{\boldsymbol{\zeta}}_{w,\mathrm{h}}$ of any element w in the healthy state is obtained as follows:

where the superscript n_1 represents any row n_1 of the transfer function matrix $\tilde{\mathbf{G}}_m$; the superscript n_0 represents any column n_0 of the transfer function matrix $\tilde{\mathbf{G}}_m$ and any row n_0 of the damage localization vector $\boldsymbol{\nu}_{\lambda,\mathrm{h}}$; and $\mathrm{D}(\tilde{y}_{\mathrm{h}}^{n_1})$ is the variance of the displacement of any DOF n_1. Similarly, according to the derivation method of Eq. (26), the variance of the stress value corresponding to the φ_0th DOF of any element w in the healthy state is calculated as shown in the following equation:

$$D\left(\xi_{w,h}^{\varphi_0}\right) = \sum_{\varphi_1=1}^{\varphi} \left\{ \left[D\left(\tilde{k}_{m,w}^{\varphi_0,\varphi_1}\right) + E\left(\tilde{k}_{m,w}^{\varphi_0,\varphi_1}\right)^2 \right] \left[D\left(\tilde{y}_{w,h}^{\varphi_0}\right) \right. \right.$$
$$\left. \left. + E\left(\tilde{y}_{w,h}^{\varphi_0}\right)^2 \right] - E\left(\tilde{k}_{m,w}^{\varphi_0,\varphi_1}\right)^2 E\left(\tilde{y}_{w,h}^{\varphi_0}\right)^2 \right\}. \quad (27)$$

On this basis, the variance of the damage location index $\tilde{\psi}_{w,h}$ in the healthy state is obtained as

$$D\left(\tilde{\psi}_{w,h}\right) = \sum_{\varphi_0=1}^{\varphi} D\left(\xi_{w,h}^{\varphi_0}\right). \quad (28)$$

The variance estimation of the damage localization index of any element in the healthy state is obtained by the above variance calculation. When the sample size of the update parameter vector and the health monitoring period are large enough, the variance estimate is considered the overall variance of the damage localization index. The variance includes not only the errors of measured noise and modal parameter identification but also the temperature error of the probabilistic FEM of the bridge under this cluster. The probability distribution of the damage localization index $\tilde{\psi}_{w,h}$ in the healthy state is shown as follows:

$$\tilde{\psi}_{w,h} \sim \Upsilon\left[E\left(\tilde{\psi}_{w,h}\right), \sum_{\varphi_0=1}^{\varphi} D\left(\xi_{w,h}^{\varphi_0}\right) \right], \quad (29)$$

where $\Upsilon[\cdot]$ denotes a probability distribution that obeys a certain mean and variance. When the bridge structure is undamaged, $E\left(\tilde{\psi}_{w,h}\right)$ is usually not equal to 0.

4.2.2 Calculation of the damage localization index in the state inquiring damage

As noted earlier, DLVs are only affected by measured noise and modal truncation in the healthy state, and when they are treated as loads acting on the probabilistic FEM of the bridge, the damage localization index will include the error caused by temperature variations in this cluster. However, if the bridge structure is damaged in the state inquiring damage, the DLV itself is affected by temperature variations. Thus, the DLV under each monitoring period needs to be treated as a set of loads acting on the mean FEM of the bridge in the corresponding cluster, as shown in the equation below. It should be noted that when the mean of the updated parameters is brought into the FEM, the corresponding FEM is defined as the mean FEM.

$$\tilde{\mathbf{y}}_d = \mathbf{E}\left[\mathbf{G}_m(\tilde{\boldsymbol{\theta}})\right]\boldsymbol{\nu}_d, \quad (30)$$

$$\tilde{\xi}_{w,d} = \mathbf{E}\left[\mathbf{k}_{m,w}(\tilde{\boldsymbol{\theta}})\right]\tilde{\mathbf{y}}_{w,d}, \quad (31)$$

where $\mathbf{E}\left[\mathbf{G}_m(\tilde{\boldsymbol{\theta}})\right]$ and $\mathbf{E}\left[\mathbf{k}_{m,w}(\tilde{\boldsymbol{\theta}})\right]$ represent the transfer function mean matrix and element stiffness mean matrix, respectively, of the probabilistic FEM of any cluster. $\boldsymbol{\nu}_d$ is the damage localization vector generated in a certain monitoring period, and the subscript d denotes the state inquiring damage. $\tilde{\xi}_{w,d}$ denotes the stress field of any element w in the state inquiring damage.

In the state inquiring damage, if the bridge structure is damaged, the DLV is affected by the temperature variations of this cluster, which is different from the healthy state. Then, when the DLV is treated as a set of loads in the mean FEM, the damage localization index includes not only the errors of measured noise and modal truncation, but also the errors caused by temperature variations in this cluster, which is consistent with the healthy state. Therefore, if the bridge structure is damaged, according to the SDDLV theory, the mean of the damage localization index of the damaged elements is 0, and the variance of the damage localization index is approximately identical in both the healthy and damaged states, as shown in Eq. (32). The loading procedure of the DLV in both of these states is shown in Fig. 4.

$$\tilde{\psi}_{w,d} \sim \Upsilon\left[0, \sum_{\varphi_0=1}^{\varphi} D\left(\xi_{w,h}^{\varphi_0}\right) \right], \quad (32)$$

where $\tilde{\psi}_{w,d}$ is the damage localization index in the state inquiring damage.

4.2.3 Damage localization for any two identical bridges based on hypothesis testing

In practical engineering applications, considering the effect of uncertain factors, i.e., temperature variations, measured noise and modal truncation, the value of $\tilde{\psi}_{w,d}$ is generally not 0 but close to 0. Since the variance of $\tilde{\psi}_{w,d}$ was obtained in the previous section, the thresholds of damage localization can be determined based on the PauTa criterion. On this
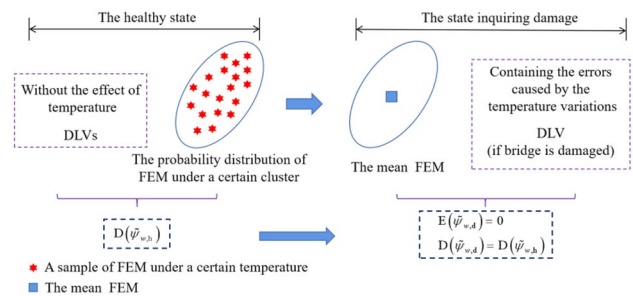

Fig. 4 Schematic diagram of the calculation procedure of the damage localization index in two states

basis, the hypothesis test below is performed to localize the damage.

$$\begin{cases} \mathbf{H}_0 : \ |\tilde{\psi}_{w,\mathrm{d}}| \ > \ 3\sqrt{\mathrm{D}(\tilde{\psi}_{w,\mathrm{h}})} \ \text{Element } w \text{ is undamaged} \\ \mathbf{H}_1 : \ |\tilde{\psi}_{w,\mathrm{d}}| \ \leq \ 3\sqrt{\mathrm{D}(\tilde{\psi}_{w,\mathrm{h}})} \ \text{Element } w \text{ is damaged} \end{cases}.$$
(33)

According to Eq. (33), it is determined whether any element of any two identical bridges is in the healthy state.

Although the damage condition can be distinguished when $\mathbf{H}_1$ is established, $\tilde{\psi}_{w,\mathrm{d}}$ does not necessarily conform to a normal distribution, and there may be type I errors in this hypothesis test. Therefore, the data of multiple monitoring periods under the state inquiring damage are further used to verify the damage condition. The damage discriminant index z_τ is defined here. When $\mathbf{H}_1$ is true in this monitoring period, z_τ is set to 1; otherwise, z_τ is set to 0, where τ denotes a certain monitoring period in the state inquiring damage. On this basis, the cumulative value Ξ_d of the damage discrimination index of any element is calculated.

$$\Xi_\mathrm{d} = \sum_{\tau=1}^{e_\mathrm{d}} z_\tau,$$
(34)

where e_d is the total number of monitoring periods in the state inquiring damage. The cumulative value Ξ_d follows a binomial distribution. Therefore, the inverse cumulative distribution function of the binomial distribution is used to calculate the cumulative threshold for localizing the damage of any element, as shown in the following equation:

$$P = \sum_{\pi=0}^{Q} \frac{e_\mathrm{d}!}{\pi! \cdot (e_\mathrm{d} - \pi)!} \ell^\pi \ell(1-\ell)^{e_\mathrm{d}-\pi},$$
(35)

where P is the probability that there are Q successes in e_d trials based on the given success rate $(1-\ell)$. ℓ is the probability of occurrence of a type I error, which is determined according to the actual situation of bridges. The value Q is the cumulative threshold for damage localization for any element. If $\Xi_{\mathrm{d},w} > Q_w$, then element w is damaged; otherwise, element w is healthy.

4.3 Damage decision for all bridges based on a cross-validation strategy

The method proposed in the previous section can only determine whether the two bridges involved in the calculation are damaged. Thus, the idea of a cross-validation strategy is implemented to determine all damaged regions of all bridges. The damage determination procedure comprises the following steps: first, one of the bridges monitored in the cluster is randomly selected as the reference bridge; second, utilizing

the method proposed above, the condition of two bridges is diagnosed using the monitoring data obtained from the reference bridge and any other bridge, and this procedure is repeated until all the structural conditions of the other bridges are diagnosed completely; third, the reference bridge is cyclically exchanged until all the bridges have been selected as the reference bridge once. Through this procedure, the response information of all bridges is integrated so that all damaged bridges and regions can ultimately be determined.

Assuming that there are N bridges with the same structural design monitored within one cluster, the cross-localization result matrix $\mathbf{R}_w$ of any element w is defined as:

$$\mathbf{R}_w = \begin{bmatrix} R_w^{2,1} & R_w^{3,1} & \cdots & R_w^{i,1} & \cdots & R_w^{N,1} \\ R_w^{1,2} & R_w^{3,2} & \cdots & R_w^{i,2} & \cdots & R_w^{N,2} \\ \vdots & \vdots & \ddots & \vdots & \cdots & \vdots \\ R_w^{1,j} & R_w^{2,j} & \cdots & R_w^{i,j} & \cdots & R_w^{N,j} \\ \vdots & \vdots & \ddots & \vdots & \ddots & \vdots \\ R_w^{1,N} & R_w^{2,N} & \cdots & R_w^{i,N} & \cdots & R_w^{N-1,N} \end{bmatrix},$$
(36)

where $R_w^{i,j}$ represents the damage localization result of any element w of bridge i when bridge j is selected as the reference bridge. If the two bridges are healthy, then $R_w^{i,j} = 1$; if element w of a bridge is damaged, then $R_w^{i,j} = 0$. On this basis, the damage decision value of any element w of bridge j is defined as follows:

$$\Phi_w^j = \frac{1}{N-1} \cdot \sum_{i \in \Theta} R_w^{i,j} \ \ (i \neq j),$$
(37)

where Θ represents the set of all bridges monitored in one cluster. If $\Phi_w^j = 0$, element w of bridge j is damaged, and if $\Phi_w^j > 0$, element w of bridge j is healthy. Based on the cross-validation strategy, the damage of all bridges is localized; meanwhile, the misjudgment of the structural damage is avoided, and the accuracy of the algorithm is improved. According to the proposed algorithm, at least three identical bridges monitored within one cluster are needed to complete the damage localization for all bridges.

5 Numerical example

5.1 Description of the numerical model and damage cases

To verify the validity and dependability of the proposed method, four three-span continuous beam models with the same structural design are established to simulate actual bridges monitored within one cluster. As shown in Fig. 5, each bridge has 3 spans and is discretized with 30 equal-sized beam elements. Vertical supports (*Z* direction) and horizontal supports (*Y* direction) are simulated using spring
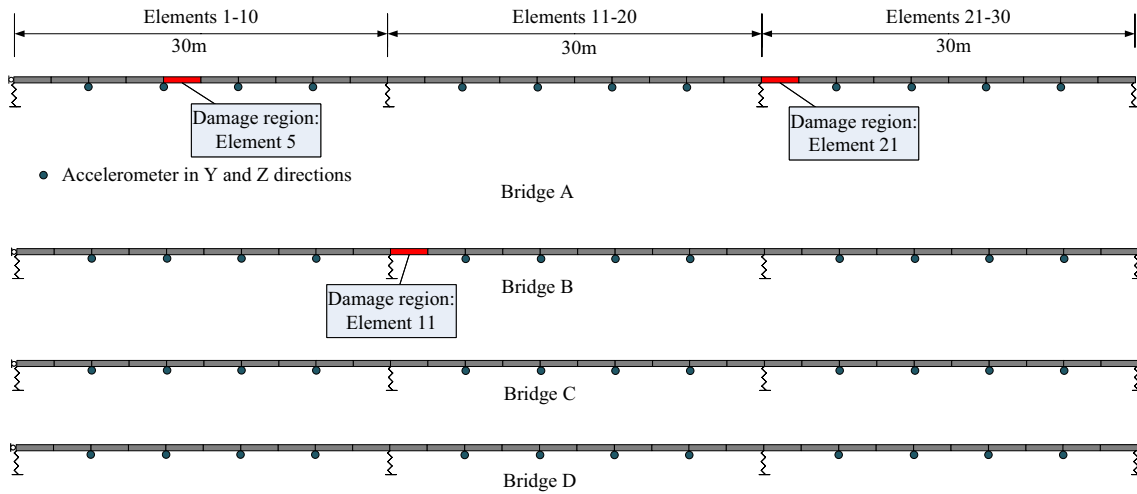
Fig. 5 Beam bridge structures monitored in one cluster

Fig. 6 Relationship between the Young modulus of the main beam material, the support stiffness and the temperature
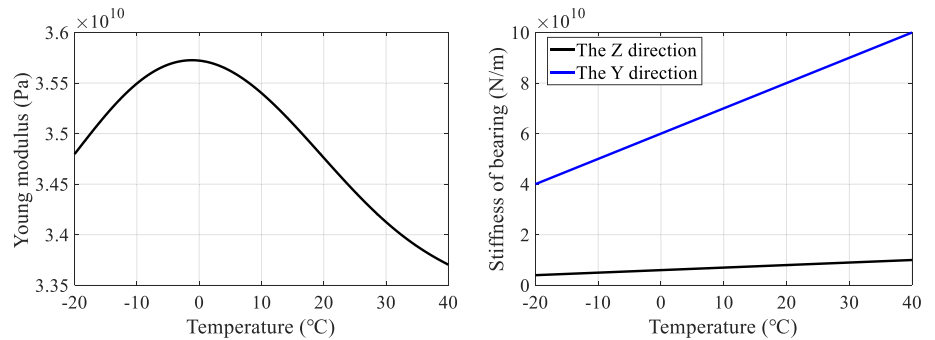
Table 1 Parameters of the FEM of the bridge structures

Parameter	Value
Poisson's ratio of the main beam material	0.2
Unit weight of the main beam material (N/m^3)	25,000
Area of the cross-section (m^2)	0.56
Moment of inertia I_z (m^4)	0.0971
Moment of inertia I_y (m^4)	0.0691
Moment of inertia I_x (m^4)	0.1195

Fig. 7 Simulated temperature variations

elements. The Young modulus of the FEM material and the stiffness of the support are related to the environmental temperature, as shown in Fig. 6 [43, 49], and the other detailed parameters are shown in Table 1. To add the effect of environmental temperature to the FEM, a total of 2190 temperature samples are generated to simulate the environmental temperature variations in one year, as shown in Fig. 7. In the simulation process for the environmental temperature, the annual air temperature variations and the daily air temperature fluctuation are considered simultaneously so that the simulated variation in the air temperature

is close to the real conditions [50]. When each temperature sample is treated as a load in the FEM, 40,000 acceleration data samples are extracted from each monitoring position under white noise excitation. The monitoring positions of the sensors are shown in Fig. 5. Thus, in the healthy state,

Table 2 Damage cases

Damage case	Damaged bridge	Damaged element	Damage extent	Environmental temperature
1	A	# 5	5%	30℃
2	A	# 5	10%	30℃
3	A	# 5	15%	30℃
4	A	# 5	10%	10℃
5	A	# 5 and # 21	10%	10℃
6	A & B	A: # 5 C: # 11	10%	10℃

acceleration samples of 2190 monitoring periods at different temperatures are obtained.

In the state inquiring damage, a total of six damage cases are set according to the different damaged bridges, damage locations, damage degrees and environmental temperatures, as shown in Table 2. A decrease in the bending stiffness (Young modulus of the material) in a local region is implemented to simulate damage phenomena, such as concrete strength reduction, the concrete spalling of superstructure of bridge, the crack of concrete, the exposure and corrosion of reinforced, the wet joint damage, etc. The damage location is shown in Fig. 5. The acceleration data under the different cases are obtained, and the extraction method of the acceleration data is identical to that in the healthy state.

5.2 Classification results of the DLV based on a GMM clustering analysis

In the healthy state, using the simulated acceleration monitoring data of bridge A, a total of 2190 sets of natural frequency samples can be identified based on the Next-ERA algorithm [51]. On this basis, 2190 environmental temperature samples and natural frequency sample sets are combined into a data sample matrix based on the Gaussian mixture distribution model, and clustering analysis is performed on the sample matrix. The sample matrix is classified into 2, 3, and 4 clusters. The clustering results show that when the sample matrix is classified into 2 clusters, the probability distribution with respect to the temperature and natural frequency is close to the combination of two Gaussian distributions, and the clustering result is considered to be more reasonable.
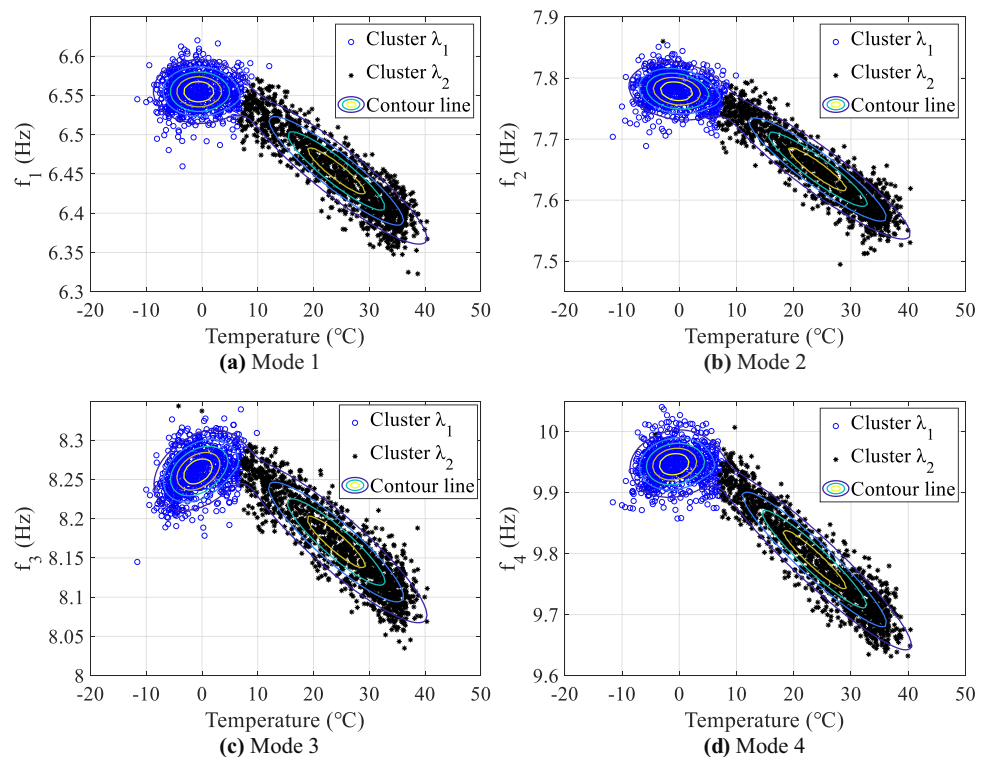
Fig. 8 Results of the clustering analysis

(a) Mode 1

(b) Mode 2

(c) Mode 3

(d) Mode 4

Table 3 Statistical characteristics of the frequencies and temperature of the two clusters

Parameters	Initial values	Values after the clustering analysis	
		Cluster λ_1 (824 samples)	Cluster λ_2 (1366 samples)
$E(T)$	15.0000	-7.4868×10^{-1}	24.4999
$E(f_1)$	6.4907	6.5547	6.4521
$E(f_2)$	7.6976	7.7786	7.6487
$E(f_3)$	8.2029	8.2610	8.1678
$E(f_4)$	9.8450	9.9463	9.7839
$Var(f_1)$	4.3005×10^{-3}	4.5014×10^{-4}	2.6575×10^{-3}
$Var(f_2)$	6.7066×10^{-3}	6.2504×10^{-3}	4.0184×10^{-3}
$Var(f_3)$	4.2950×10^{-3}	7.0610×10^{-4}	3.1960×10^{-3}
$Var(f_4)$	1.0391×10^{-2}	8.4321×10^{-4}	6.2242×10^{-3}
$Cov(f_1, f_2)$	4.8375×10^{-3}	-2.1447×10^{-5}	2.7473×10^{-3}
$Cov(f_1, f_3)$	3.7436×10^{-3}	1.8902×10^{-5}	2.3923×10^{-3}
$Cov(f_1, f_4)$	6.1140×10^{-3}	5.2021×10^{-5}	3.4963×10^{-3}
$Cov(f_2, f_3)$	4.6896×10^{-3}	-2.3166×10^{-6}	2.9644×10^{-3}
$Cov(f_2, f_4)$	7.6761×10^{-3}	3.9325×10^{-5}	4.3389×10^{-3}
$Cov(f_3, f_4)$	5.9352×10^{-3}	8.4256×10^{-5}	3.7723×10^{-3}

The clustering results are shown in Fig. 8. The statistical characteristics of the natural frequencies and temperature of the two clusters are listed in Table 3.

Based on the statistical characteristics of the natural frequencies and temperatures of the two clusters, it is concluded that the covariance of the natural frequencies of each cluster decreases significantly after clustering, indicating that the establishment of a probabilistic FEM based on the natural frequency after clustering will greatly reduce the effect of the temperature.

According to the clustering results for the temperature, the DLVs obtained during the 2190 monitoring periods based on the monitoring data of bridges A and B are also classified into two clusters in the healthy state. The DLVs generated below 7.0451℃ are classified into one cluster, and the DLVs generated above 7.0451℃ are classified into the other cluster. The classification results of the DLVs are divided into two categories, winter and summer, and the natural frequency values of both clusters conform to approximately the same probability distribution.

5.3 Establishment of the probabilistic FEMs of a bridge

According to the clustering results of the natural frequencies, the probabilistic FEM of each cluster is established. The structural size of the original FEM before updating is consistent with the FEM of the simulated bridges in the previous section. The difference is that the initial Young modulus of the main beam material is set to 3.35×10^4 MPa; the initial support stiffness in the Z direction and Y direction are set to 5×10^9 N/m and 5×10^{10} N/m, respectively. The update parameters are defined as θ_1, θ_2, and θ_3, which are the coefficients of the Young modulus of the material of the main beam, the support stiffness in the Z direction, and the support stiffness in the Y direction, respectively. Therefore, the update parameters are affected by temperature variations. The initial values of the update parameters are set to 1, as shown in Table 4.

The probabilistic FEM updating method proposed in [6] is adopted to update the mean $\mathbf{E}(\boldsymbol{\theta})$ and covariance $\mathbf{Cov}(\boldsymbol{\theta})$ of the update parameters in this study. Under each cluster, a genetic algorithm (GA) [52] is used for optimization. According to the mean and covariance of the updated parameters after each iteration, the Monte Carlo simulation method is used to generate 1000 updated samples, which are then used in the FEM to calculate the analytical value of the natural frequency for each sample. Finally, the update procedure of the model is completed by minimizing the optimization parameters constructed according to the simulated natural frequency and the analytical value of the natural frequency, which is described in detail in [6]. The statistical values of the update parameters before and after the FEM updating are shown in Table 5. Based on the updated mean and covariance of the update parameters, the mean and variance of each element in the transfer function matrix $\mathbf{G}_m(\tilde{\boldsymbol{\theta}})$ and element stiffness matrix $\mathbf{k}_{m,w}(\tilde{\boldsymbol{\theta}})$ are calculated by Eqs. (31)–(35).

To reflect the accuracy of the probabilistic FEM, the distribution diagram of the first and fourth natural frequencies before and after the FEM updating in two clusters is shown in Fig. 9. With FEM updating, the difference between the distributions of the analytical and simulated natural frequencies is greatly reduced, which reflects the accuracy of the probabilistic FEM.

Table 4 Initial values of the update parameters

Parameters	Elastic modulus of the main beam material (MPa)	Support stiffness in the Z direction (N/m)	Support stiffness in the Y direction (N/m)
Values	$\theta_1 \times 3.35 \times 10^4$ (Initial value of θ_1 is 1)	$\theta_2 \times 5 \times 10^9$ (Initial value of θ_2 is 1)	$\theta_3 \times 5 \times 10^{10}$ (Initial value of θ_3 is 1)

Table 5 The statistical values of the updating parameters before and after FEM updating

Statistical value	Cluster λ_1		Cluster λ_2	
	Initial value	After updating	Initial value	After updating
$E(\theta_1)$	1.0000	1.0571	1.0000	1.0221
$E(\theta_2)$	1.0000	1.1678	1.0000	1.6601
$E(\theta_3)$	1.0000	1.1130	1.0000	1.6680
$Var(\theta_1)$	3.0107×10^{-5}	4.7311×10^{-5}	2.6600×10^{-4}	1.8308×10^{-4}
$Var(\theta_2)$	4.7521×10^{-2}	6.8527×10^{-2}	4.6813×10^{-2}	4.6743×10^{-2}
$Var(\theta_3)$	2.0592	2.6857	2.0454	3.0708
$Cov(\theta_1, \theta_2)$	-7.9959×10^{-4}	-1.1129×10^{-3}	-1.5915×10^{-3}	-1.6088×10^{-3}
$Cov(\theta_1, \theta_3)$	-5.3675×10^{-3}	-6.9946×10^{-3}	-5.5856×10^{-3}	-8.4466×10^{-3}
$Cov(\theta_3, \theta_4)$	1.6235×10^{-1}	2.1122×10^{-1}	1.5401×10^{-1}	2.33039×10^{-1}

Fig. 9 Comparison of the distributions of the natural frequency before and after FEM updating

(a) Cluster λ_1

(b) Cluster λ_2
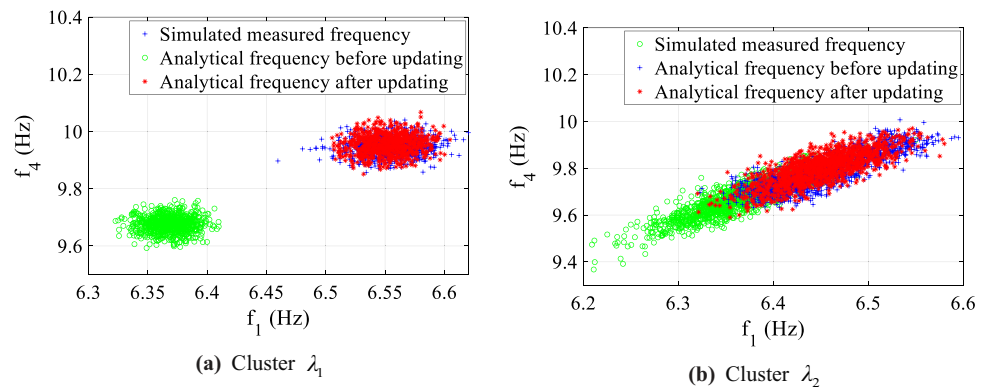
Table 6 Damage cases

Damage cases	Damage element	Damage location	Damage extent (%)	Noise level (%)
1	#14- #16	The mid-span of the second span side beam	5	5
2	#14- #16	The mid-span of the second span side beam	10	5
3	#14- #16	The mid-span of the second span side beam	15	Ffig 5

5.4 Comparison of the performance of the proposed method and the conventional SDDLV method

5.4.1 Comparison of the damage localization results without noise effects

To verify the effectiveness of the proposed method under the effect of environmental temperature, numerical simulation data without noise effects are used in this section to compare the proposed method and the conventional SDDLV method. In the conventional SDDLV method, when the DLV is treated as a set of loads acting on the undamaged FEM, the weighted stress index (WSI) value of all elements needs to be calculated [16]. When the WSI value of any element is less than 1, this indicates that the element is a candidate for damage.

Bridge C is selected as the reference bridge. In the damage localization results without considering environmental temperature variations, the undamaged FEM before updating is used to calculate the stress on all the elements of the bridges, and the healthy state of the bridge is the state corresponding to 0 °C. The comparison results of the damage localization of the bridge in cases 1–5 are shown in Fig. 10.
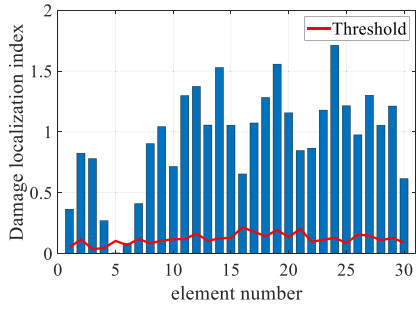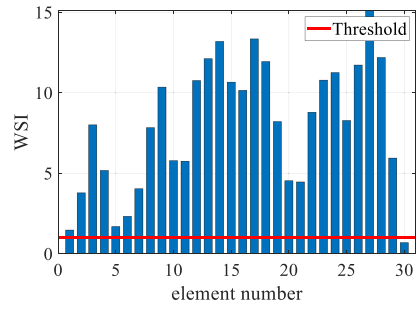
Figure 10a–c show that when the temperature is 30 °C in the damaged state, the proposed method can effectively localize the structural damage of element 5 in cases 1–3 after considering the environmental temperature variations. However, the SDDLV method, which does not consider the temperature variations, cannot localize
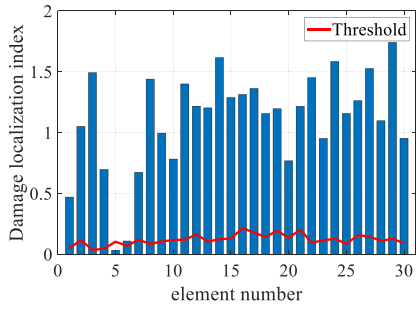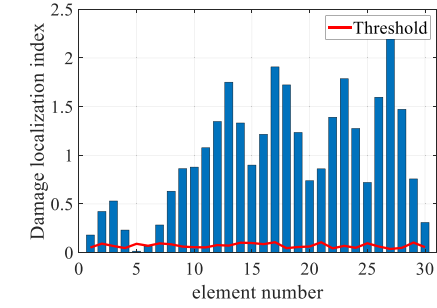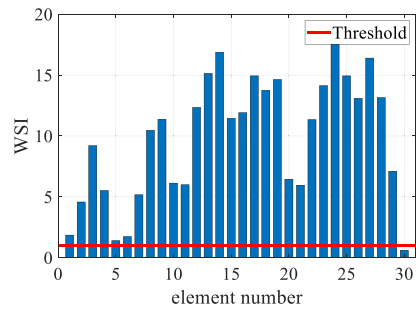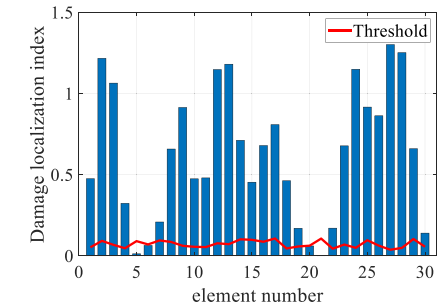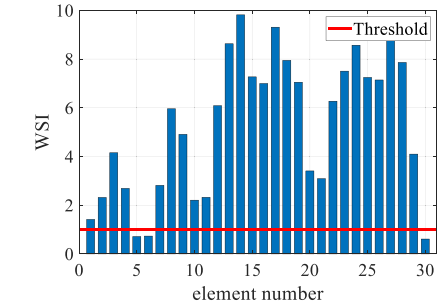
(a) Case 1
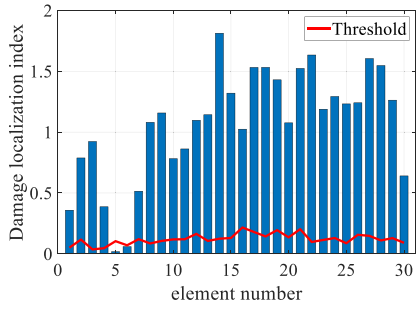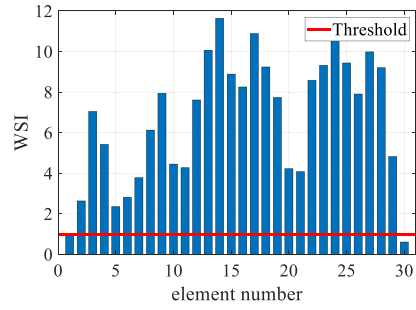
(b) Case 2
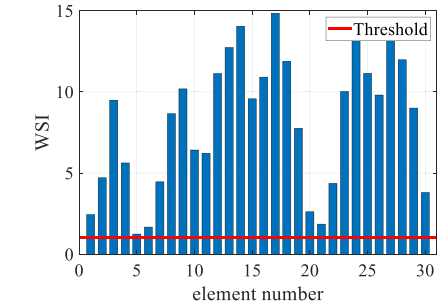
(c) Case 3

(d) Case 4

(e) Case 5

◀**Fig. 10** Comparison of the damage localization results for bridge structure. (The left side is the result of the proposed method, and the right side is the result of the conventional SDDLV method.)

the structural damage of element 5 and misjudges other undamaged elements. Thus, when the difference in temperature between the healthy state and the damaged state is large, structural damage at the level of 15% cannot be effectively localized. Figure 10d shows that when the temperature is 10℃ in the damaged state and the damage degree of the element is 10%, the SDDLV method that does not consider the temperature variations can localize the structural damage of element 5, but the WSI value of the damaged element is close to the empirical threshold, and other elements still show misjudgment phenomenon. Therefore, if the damage degree is small, the effectiveness of damage localization will be greatly reduced, which further verifies that the environmental temperature has a great impact on the damage localization results. Figure 10e shows that when damage occurs simultaneously in elements 5 and 11, the proposed method still shows accurate structural damage localization, and the effectiveness of the damage localization is poor if the influence of temperature is not considered.

5.4.2 Comparison of the damage localization results considering noise effects

For the damage localization results in case 4, it is obvious that when the environmental temperature and noise are not considered in the conventional SDDLV method, the WSI value of element 5 is close to the empirical threshold. Therefore, in this section, the damage localization results of case 4 based on both the proposed method and the conventional SDDLV method are compared under different levels of noise.

For case 4 (the temperature is 10 °C, and the damage degree of element 5 is 10%), a total of 300 sets of acceleration data are simulated under the influence of 5% and 10% noise. The FEM of the bridge is the same as in the previous section. Damage localization for the bridge is performed using each set of acceleration data, and the cumulative damage discrimination index is calculated. The comparison results of the noise resistance performance are shown in Fig. 11. Figure 11b shows that the structural damage of element 5 of bridge A is effectively localized under the effect of 10% noise using the proposed method. Figure 11a shows that the damage of element 5 cannot be localized after adding 5% noise using the conventional SDDLV method, which does not consider the effect of temperature variations.

5.5 Results of damage cross-localization between bridges

In this section, a cross-validation strategy is applied to localize the damage of all bridges monitored within one cluster. Bridges A, B, C and D are selected as reference bridges. Through the damage localization method proposed in this study, the damage condition of any element of the reference bridge and any other bridge can be identified. On this basis, the reference bridge is cyclically exchanged until all bridges have been used as reference bridges.

For case 6 (element 5 of bridge A and element 11 of bridge B are damaged), the damage cross localization results of all bridges are shown in Fig. 12. Figure 12a–d show the R values of all elements when bridges A, B, C and D are selected as the reference bridge. Then, the damage decision value of each bridge is obtained as follows: (1) Bridge A: $\lambda_5^A = 0$, $\lambda_{others}^A > 0$; (2) Bridge B: $\lambda_{11}^B = 0$, $\lambda_{others}^B > 0$; (3) Bridge C: $\lambda_{all}^C > 0$; (4) Bridge D: $\lambda_{all}^D > 0$. The results show that element 5 of bridge A and element 11 of bridge B are candidates for damage, and bridges C and D are healthy. The decision results of the damage are consistent with the damage setting, and through the cross-validation of all bridges monitored within one cluster, accidental misjudgments are effectively avoided.

6 Analysis of the effect of structural deviations in construction

In this section, acceleration monitoring data obtained from a structural health monitoring (SHM) system for actual bridges are applied to verify the performance of the proposed method under the effect of structural deviations in construction. Figure 13 shows the overall diagram of all bridges monitored within one cluster, which is the Shunhe Bridge located in Jinan, China. Since the operating time of the bridge is relatively short and there is no substantial damage, this section will focus on the analysis of the effect of structural deviations in construction between the same bridges on the damage localization results.

6.1 Description of the SHM systems of bridges monitored within one cluster

The acceleration monitoring data from bridges A and B were selected for analysis and verification. Both bridges are 3 × 30 m continuous beam bridges with a single box and five chambers. Figure 14 shows the layout of the acceleration sensors of the two bridges, in which monitoring
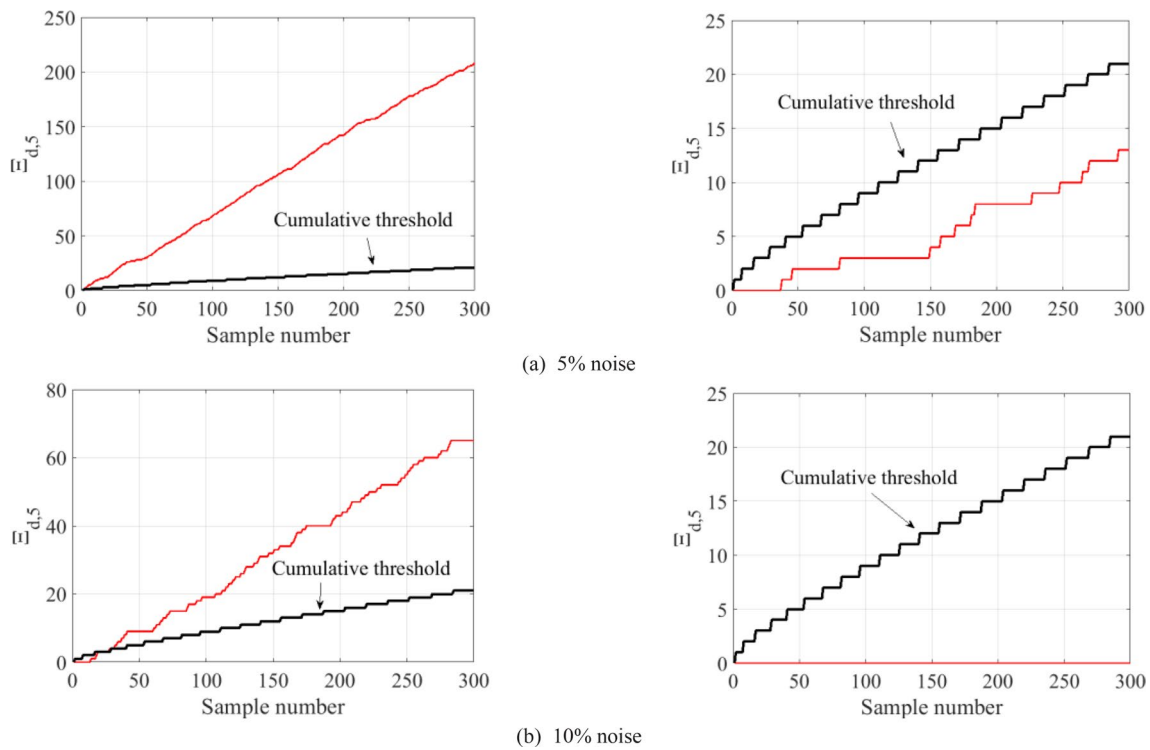
(a) 5% noise

(b) 10% noise

Fig. 11 The comparison results of the noise resistance performance. (The left side is the proposed method, and the right side is the conventional SDDLV method.)
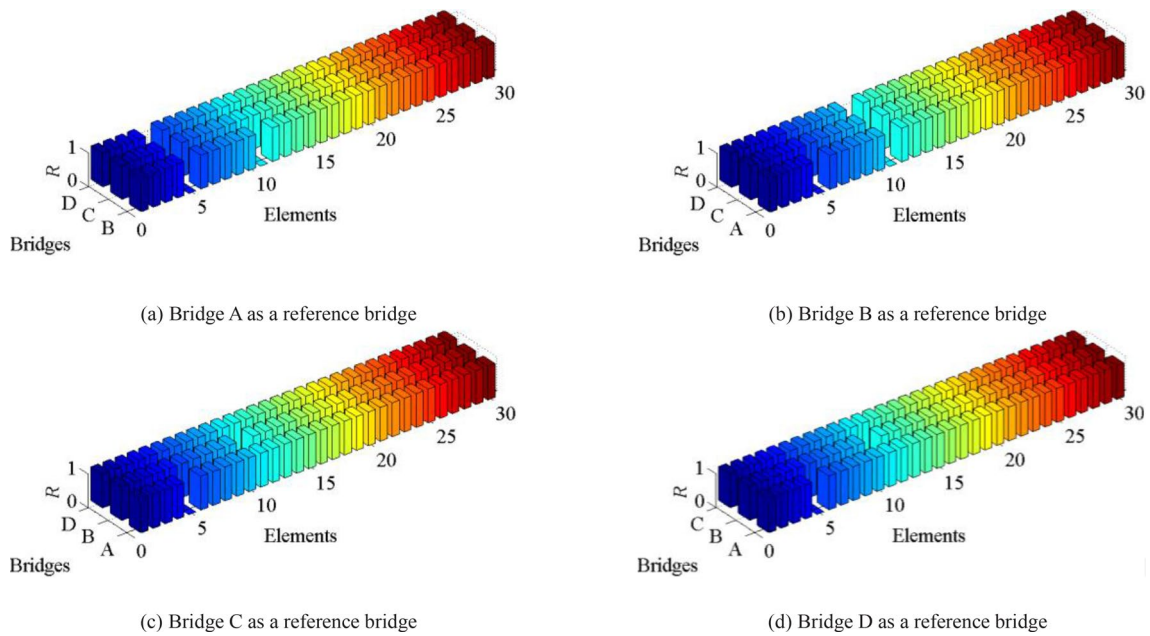

(a) Bridge A as a reference bridge

(b) Bridge B as a reference bridge

(c) Bridge C as a reference bridge

(d) Bridge D as a reference bridge

Fig. 12 Damage cross-localization results of all bridges

sections are set at the mid-span and 1/4 section of the first and second spans, and a total of six monitoring sections are set in each bridge, as shown in Fig. 14a. Three

acceleration sensors are installed in the first, third and fifth chambers of each monitoring section, as shown in Fig. 14b. Figure 15 shows the field installation of the

Fig. 13 Photograph of the actual bridges

(a) Vertical section layout

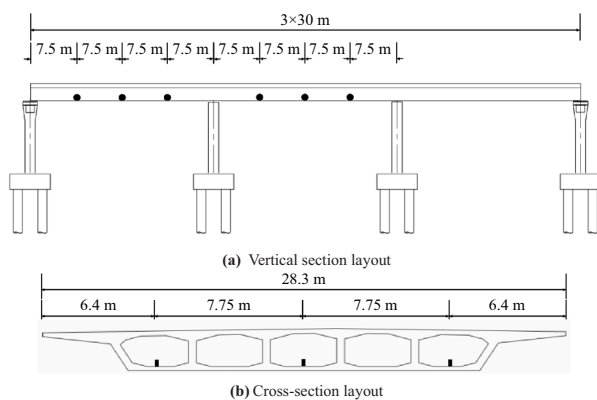**(b)** Cross-section layout

Fig. 14 Placement of the acceleration sensors

acceleration monitoring system for the bridges monitored in the cluster. The sampling frequency of the acceleration sensors is 200 Hz.

All bridges are located in the same traffic route, and there is no traffic confluence or diversion. Therefore, the traffic loads of all the bridges are basically equal.
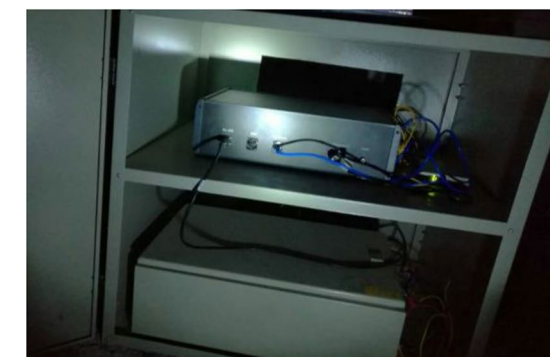
Furthermore, the effect of light on each bridge is similar, and the environmental temperature load is also similar. The SHM systems began to collect strain monitoring data in June 2016. There was no vehicle load on the bridge from June 2016 to April 2017, and the bridges were officially opened to traffic in May 2017.

6.2 An analytical method combining the simulated and measured data

The difference in the transfer function matrix between two identical bridges can be obtained for the same period, and then the DLV is generated for each monitoring period. However, bridges with the same structural design often have certain structural deviations in construction. To analyze the effect of the structural deviations in construction, an analysis method combining the simulated and measured data is proposed in this section. The analysis steps are as follows:

Step 1: According to the design size of two actual identical bridges monitored within one cluster, the definite FEM of the bridges is established.

Step 2: The actual natural frequency monitoring data and temperature monitoring data are clustered, and the probability FEM of each cluster is established according to the clustering results.

Step 3: A sample of the updated parameters is brought into the FEM. According to the actual positions of the monitoring sensors of the two bridges, the acceleration data in the healthy and damaged states are obtained under noise excitation.

Step 4: When $\Delta\mathbf{R}$ is constructed using each set of acceleration simulation data, the statistical mean of $\Delta\mathbf{R}_a$ under all monitoring periods is added to $\Delta\mathbf{R}$. In this case, the structural deviations in construction between the actual bridges are added to the simulation data, as shown in the following equation:
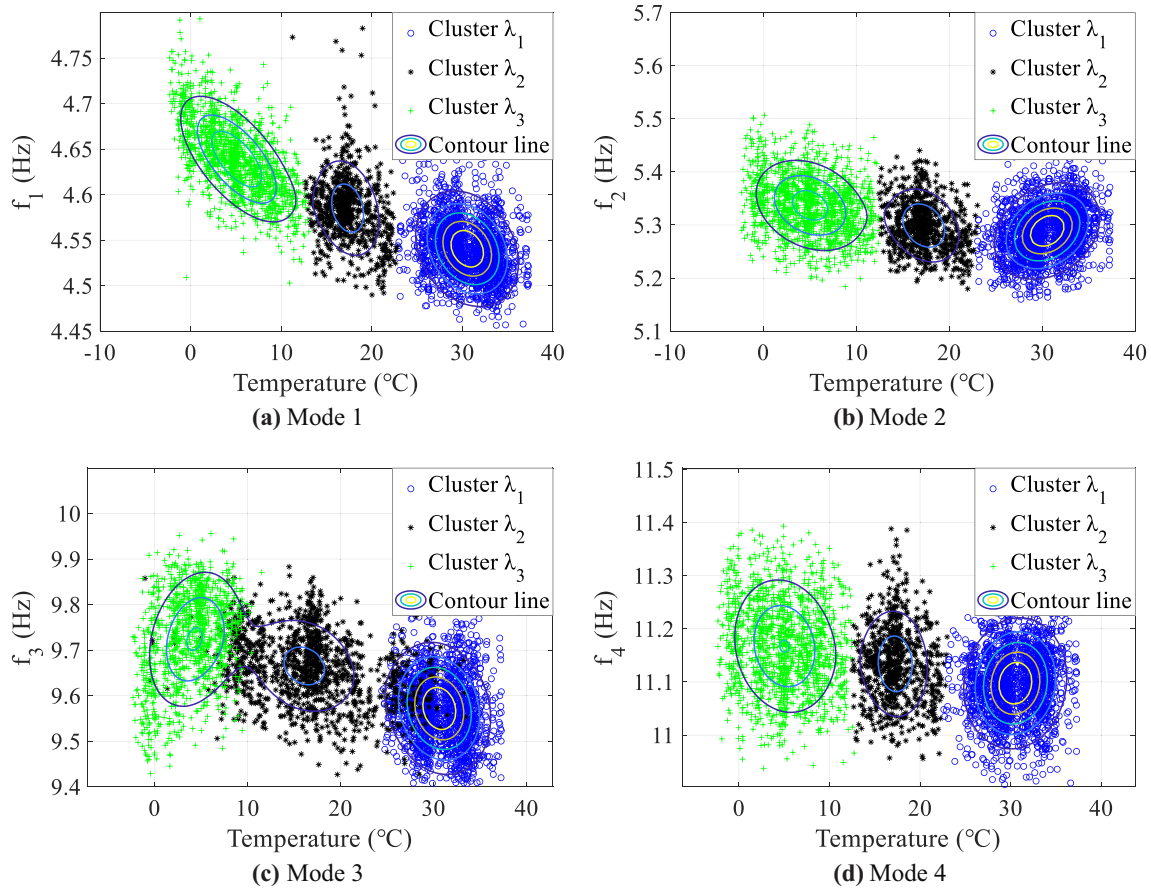

(a) Acceleration sensor

(b) Data acquisition instrument

Fig. 15 Field installation of the SHM systems

Fig. 16 Clustering results of the measured natural frequency data

$$\Delta \mathbf{R} = \Delta \mathbf{R}_s + \mathbf{E}(\Delta \mathbf{R}_a), \tag{38}$$

where $\Delta \mathbf{R}_s$ is the simulated data and $\Delta \mathbf{R}_a$ is the actual monitoring data of the two bridges.

Step 5: Using the method proposed in this study, the damage localization results before and after adding the structural deviations in construction are compared and analyzed.

6.3 Comparison results before and after adding the structural deviations in construction

In this section, the acceleration monitoring data of bridges A and B monitored within one cluster from May 2017 to April 2018 are selected for analysis. The clustering results of the measured natural frequency and temperature data are shown in Fig. 16. The clustering results show that when the sample matrix is classified into three clusters, the probability distribution with respect to the temperature and natural frequency is close to a combination of three Gaussian distributions, and the clustering result is considered to be more reasonable. Based on the design drawings of the two identical bridges A and B, the FEM of bridges is established
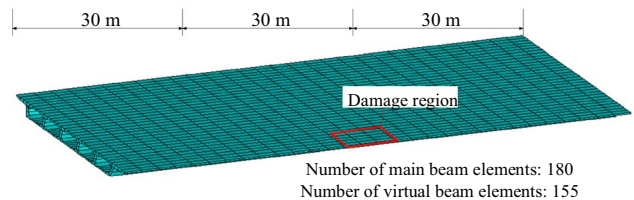

Fig. 17 FEM of the actual bridge

using the beam elements, as shown in Fig. 17. On this basis, the Young modulus of the bridge and the support stiffness in the Z direction are selected as the update parameters, and the probabilistic FEMs of different clusters are established according to the clustering results.

A sample (where the Young modulus is 3.523×10^4 MPa and the support stiffness in the Z direction is 9.839×10^8 N/m) of the updated parameters under cluster λ_1 is brought into the FEM of bridges A and B. In the healthy state, a total of 500 sets of acceleration data are generated under the excitation of environmental noise by the FEM of bridges A and B, which are used to establish
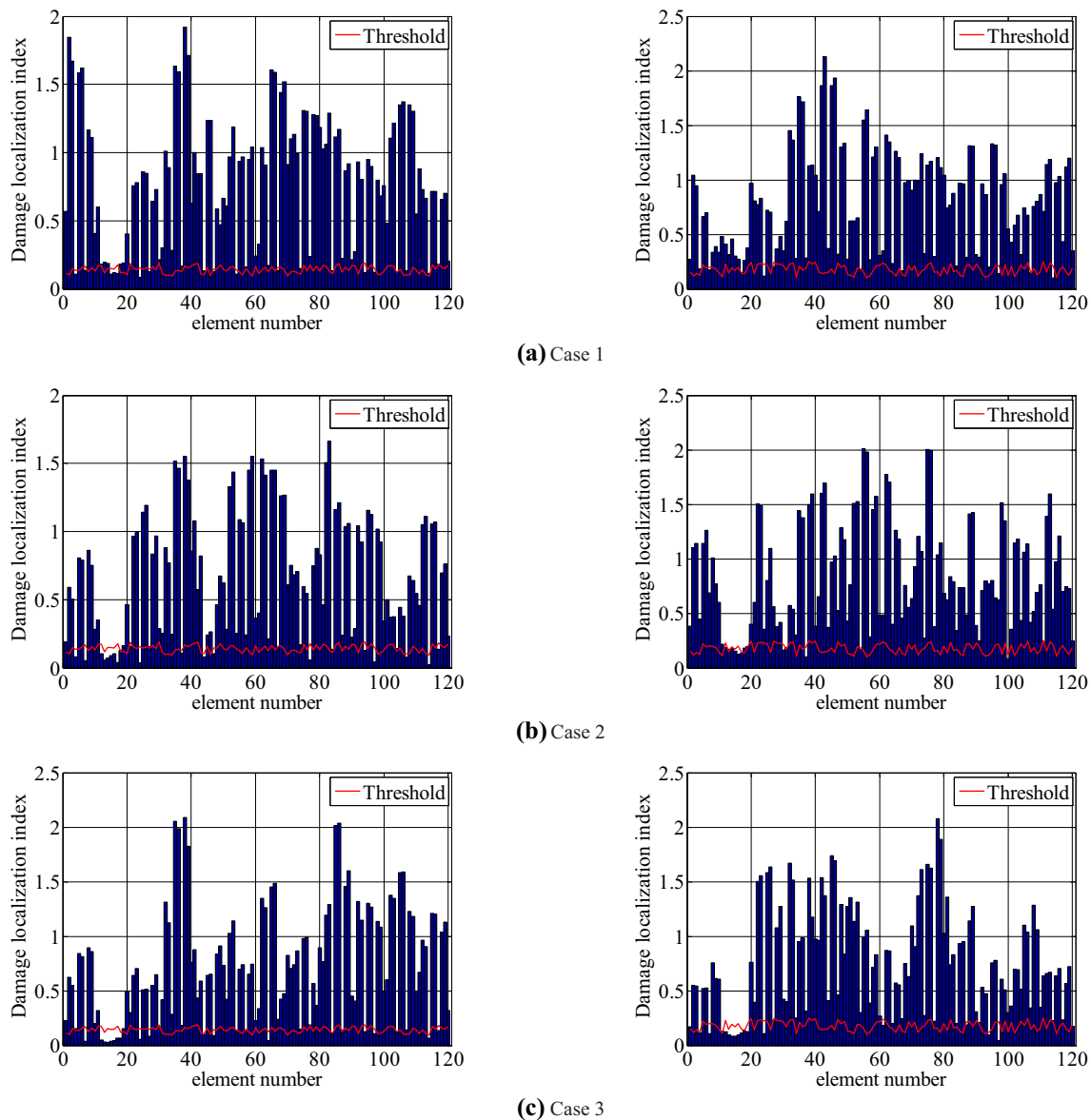
(a) Case 1

(b) Case 2

(c) Case 3

Fig. 18 Damage localization results. (The left side is the result without considering the structural deviations in construction, and the right side is the result considering the structural deviations in construction.)

the damage localization threshold. The damage cases are shown in Table 6. On this basis, the structural deviations in construction between the two actual bridges are added to the simulated data, and the algorithm proposed in this study is used to localize the damage of the two bridges. The damage localization results before and after adding the structural deviations in construction are shown in Fig. 18. Since sensors are only placed on the first two spans of the bridge structure, Fig. 18 shows only the damage localization results of the first two spans of the bridge. Figure 18 shows that (1) for the three-span continuous bridge structure, when the actual monitoring locations are relatively sparse, the localization range of the damage is accurate regarding

the vicinity of the damage location but not the specific element; (2) after adding the structural deviations in construction between the actual bridges, the damage is effectively localized for the cases with damage degrees of 10% and 15%, while the localization result for the cases with a damage degree of 5% is poor.

According to the above analysis results, when the damage degree is larger than the structural deviations in construction between the bridges in a broad sense, the proposed method can effectively localize the structural damage. Meanwhile, as construction technology progresses, the effect of structural deviations in construction between identical bridges on the proposed method will be reduced.

7 Conclusions

In this study, a probabilistic SDDLV method is proposed for damage localization for bridges monitored within one cluster under time-varying environmental temperatures. The main conclusions drawn are as follows:

(i) In the proposed method, the DLVs are generated using acceleration monitoring data acquired in the same period that are obtained from any pair of identical bridges among all the bridges monitored within one cluster. Additionally, considering the effect of temperature variations, the probabilistic FEM is established to replace the usual definite FEM. These methods can effectively mitigate the effect of temperature variations on the damage localization of all bridges.

(ii) Numerical examples show that when the temperature changes by 10℃ and the noise level is 5%, the conventional SDDLV method will lose efficacy, and it will be easy to misjudge a healthy unit. The proposed method maintains a high accuracy of damage localization under the effect of temperature variations and noise.

(iii) Using the cross-validation strategy, the structural monitoring information of all bridges is merged to determine the damage locations of all bridges monitored within one cluster and effectively avoid misjudgment.

(iv) After adding the structural deviations in construction between identical bridges into the simulation data, the localization results of different damage degrees show that structural deviations in construction reduce the accuracy of the proposed method to a certain extent. Therefore, the application condition of the proposed method is that the damage degree is larger than the structural deviations in construction between the bridges in a broad sense.

Appendix I. GMM cluster analysis process of the natural frequency and temperature monitoring data

According to Eqs. (16) and (17), $\boldsymbol{\Phi}$ is sampled from an $(m+1)$-dimensional continuous random distribution with unknown density $\eta(\boldsymbol{\Phi})$. After mixing the multivariate normal component densities, an estimate of this unknown density is obtained for a given sample.

$$\eta(\boldsymbol{\Phi}) = \sum_{\lambda=1}^{\mho} \beta_\lambda p\Big[\boldsymbol{\Phi}\Big|\mathbf{E}(\boldsymbol{\Phi}_\lambda), \mathbf{Cov}(\boldsymbol{\Phi}_\lambda)\Big], \qquad (39)$$

where $\mho$ is the mixed component of the Gaussian mixture distribution, namely, the total number of clusters, and β_λ denotes the mixing proportion of the λth cluster. Additionally, $p\Big[\boldsymbol{\Phi}\Big|\mathbf{E}(\boldsymbol{\Phi}_\lambda), \mathbf{Cov}(\boldsymbol{\Phi}_\lambda)\Big]$ is the multivariable Gaussian density of the λth cluster with mean $\mathbf{E}(\boldsymbol{\Phi}_\lambda)$ and covariance $\mathbf{Cov}(\boldsymbol{\Phi}_\lambda)$; this distribution is defined as follows:

$$\Big[\boldsymbol{\Phi}\Big|\mathbf{E}(\boldsymbol{\Phi}_\lambda), \mathbf{Cov}(\boldsymbol{\Phi}_\lambda)\Big] = \frac{1}{\sqrt{(2\pi)^{m+1}\big\|\mathbf{Cov}(\boldsymbol{\Phi}_\lambda)\big\|}}$$
$$\exp\left\{-\frac{1}{2}\big[\boldsymbol{\Phi} - \mathbf{E}(\boldsymbol{\Phi}_\lambda)\big]^\mathrm{T}\big[\mathbf{Cov}(\boldsymbol{\Phi}_\lambda)\big]^{-1}\big[\boldsymbol{\Phi} - \mathbf{E}(\boldsymbol{\Phi}_\lambda)\big]\right\}. \tag{40}$$

Assuming that all the data column vectors of the sample matrix are independent of each other, the parametric model $\big\{[\beta_\lambda, \mathbf{E}(\boldsymbol{\Phi}_\lambda), \mathbf{Cov}(\boldsymbol{\Phi}_\lambda)]|1 \le \lambda \le \mho\big\}$ is estimated by maximizing the following log-likelihood estimation from the measured data:

$$\boldsymbol{\psi}(\boldsymbol{\Phi}) = \ln\left[\prod_{g=1}^{k} \eta(\boldsymbol{\Phi}_g)\right]$$
$$= \sum_{g=1}^{k} \ln\left[\sum_{\lambda=1}^{k} \beta_\lambda p_\lambda\Big(\boldsymbol{\Phi}_g\Big|\mathbf{E}(\boldsymbol{\Phi}_\lambda), \mathbf{Cov}(\boldsymbol{\Phi}_\lambda)\Big)\right]. \tag{41}$$

The above optimization problem is solved using the expectation maximization (EM) method [53]. If the parametric model $\big\{[\beta_\lambda, \mathbf{E}(\boldsymbol{\Phi}_\lambda), \mathbf{Cov}(\boldsymbol{\Phi}_\lambda)]|1 \le \lambda \le \mho\big\}$ can maximize Eq. (41), then according to the assumption that the partial derivative of $\boldsymbol{\psi}(\boldsymbol{\Phi})$ with respect to $\mathbf{E}(\boldsymbol{\Phi}_\lambda)$ is 0, the following equation is obtained:

$$\sum_{g=1}^{k} \frac{\beta_\lambda p_\lambda\Big[\boldsymbol{\Phi}_g\Big|\mathbf{E}(\boldsymbol{\Phi}_\lambda), \mathbf{Cov}(\boldsymbol{\Phi}_\lambda)\Big]}{\sum\limits_{\lambda=1}^{\mho} \beta_\lambda p_\lambda\Big[\boldsymbol{\Phi}_g\Big|\mathbf{E}(\boldsymbol{\Phi}_\lambda), \mathbf{Cov}(\boldsymbol{\Phi}_\lambda)\Big]}\big[\boldsymbol{\Phi}_g - \mathbf{E}(\boldsymbol{\Phi}_\lambda)\big] = 0. \tag{42}$$

Solving Eq. (42), one obtains

$$\mathbf{E}(\boldsymbol{\Phi}_\lambda) = \sum_{g=1}^{k} \gamma_{g,\lambda}\boldsymbol{\Phi}_g \bigg/ \sum_{g=1}^{k} \gamma_{g,\lambda}, \tag{43}$$

where $\gamma_{g,\lambda}$ denotes the posterior probability of sample $\boldsymbol{\Phi}_g$, which is generated through the λth Gaussian mixture distribution, as shown in Eq. (44).

$$\gamma_{g,\lambda} = \frac{\beta_\lambda p\Big[\boldsymbol{\Phi}_g\Big|\mathbf{E}(\boldsymbol{\Phi}_\lambda), \mathbf{Cov}(\boldsymbol{\Phi}_\lambda)\Big]}{\sum\limits_{\lambda=1}^{\mho} \beta_\lambda p\Big[\boldsymbol{\Phi}_g\Big|\mathbf{E}(\boldsymbol{\Phi}_\lambda), \mathbf{Cov}(\boldsymbol{\Phi}_\lambda)\Big]}. \tag{44}$$

Similarly, according to the assumption that the partial derivative of $\boldsymbol{\psi}(\boldsymbol{\Phi})$ with respect to $\mathbf{Cov}(\boldsymbol{\Phi}_\lambda)$ is 0, one obtains

$$\mathbf{Cov}(\mathbf{\Phi}_\lambda) = \left\{ \sum_{g=1}^{k} \gamma_{g,\lambda} [\mathbf{\Phi}_g - \mathbf{E}(\mathbf{\Phi}_\lambda)][\mathbf{\Phi}_g - \mathbf{E}(\mathbf{\Phi}_\lambda)]^T \right\} \Big/ \sum_{g=1}^{k} \gamma_{g,\lambda}.$$

(45)

Regarding the mixing proportion β_λ, in addition to maximizing $\mathbf{\psi}(\mathbf{\Phi})$, the conditions $\beta_\lambda \geq 0$ and $\sum_{\lambda=1}^{k} \beta_\lambda = 1$ should also be satisfied. β_λ is calculated by the equation below; namely, the mixing proportion of each Gaussian component is determined by the average posterior probability of the monitored sample belonging to that component.

$$\beta_\lambda = \frac{1}{k} \sum_{g=1}^{k} \gamma_{g,\lambda}.$$

(46)

With the cluster analysis method based on the GMM, both the temperature and natural frequency data in each monitoring period are classified into different clusters. For each cluster, the natural frequencies satisfy the same probability distribution, reflecting a similar environmental effect on the structural stiffness.

Appendix II. Calculation of statistical parameters of probabilistic FEM

The global stiffness matrix $\mathbf{K}_m(\tilde{\mathbf{\theta}})$ and transfer function matrix $\mathbf{G}_m(\tilde{\mathbf{\theta}})$ of the FEM of a bridge can be regarded as functions of the random variable $\tilde{\mathbf{\theta}}$; therefore, each of their terms is also a random variable. The global stiffness matrix of the FEM of a bridge is transformed into a vector, as shown below

$$\mathbf{\underset{\sim}{K}}_m(\tilde{\mathbf{\theta}}_k) = \mathbf{vec}[\mathbf{K}_m(\tilde{\mathbf{\theta}}_k)],$$

(47)

where $\mathbf{K}_m(\tilde{\mathbf{\theta}}_k)$ is the global stiffness matrix of the FEM of the bridge corresponding to the kth sample of the updated parameters and $\mathbf{vec}(\cdot)$ is the vectorization operator that stacks the columns of a matrix into a vector.

Using the first-order Taylor series, $\mathbf{K}_m(\tilde{\mathbf{\theta}}_k)$ is approximately expressed as follows:

$$\mathbf{\underset{\sim}{K}}_m(\tilde{\mathbf{\theta}}_k) = \mathbf{\underset{\sim}{K}}_m[\mathbf{E}(\tilde{\mathbf{\theta}})] + [\tilde{\mathbf{\theta}}_k - \mathbf{E}(\tilde{\mathbf{\theta}})] \cdot \mathbf{N}_\theta[\mathbf{E}(\tilde{\mathbf{\theta}})],$$

(48)

where $\mathbf{E}(\tilde{\mathbf{\theta}})$ is the mean vector of the updated parameters, $\mathbf{E}(\tilde{\mathbf{\theta}}) \in \mathbb{R}^{1 \times v}$; for the sake of simplicity, the random variable $\tilde{\mathbf{\theta}}$ omits the expressions of all clusters λ; and $\mathbf{N}_\theta[\mathbf{E}(\tilde{\mathbf{\theta}})]$ is the sensitivity matrix of $\mathbf{\underset{\sim}{K}}_m(\tilde{\mathbf{\theta}}_k)$ with respect to $\mathbf{E}(\tilde{\mathbf{\theta}})$, $\mathbf{N}_\theta[\mathbf{E}(\tilde{\mathbf{\theta}})] \in \mathbb{R}^{v \times n^2}$, which is obtained using the sensitivity calculation method based on complex perturbation [54]. The calculation procedure is described in the Appendix III.

According to Eq. (48), the mean vector of $\mathbf{\underset{\sim}{K}}_m(\tilde{\mathbf{\theta}})$ is calculated as follows:

$$\mathbf{E}\left[\mathbf{\underset{\sim}{K}}_m(\tilde{\mathbf{\theta}})\right] = \frac{1}{r} \sum_{k=1}^{r} \left\{ \mathbf{\underset{\sim}{K}}_m[\mathbf{E}(\tilde{\mathbf{\theta}})] + [\mathbf{\theta}_k - \mathbf{E}(\tilde{\mathbf{\theta}})] \cdot \mathbf{N}_\theta[\mathbf{E}(\tilde{\mathbf{\theta}})] \right\}$$

$$= \mathbf{\underset{\sim}{K}}_m[\mathbf{E}(\tilde{\mathbf{\theta}})] + \left[\frac{1}{r} \sum_{k=1}^{r} \tilde{\mathbf{\theta}}_k - \mathbf{E}(\tilde{\mathbf{\theta}}) \right] \cdot \mathbf{N}_\theta[\mathbf{E}(\tilde{\mathbf{\theta}})]$$

$$= \mathbf{\underset{\sim}{K}}_m[\mathbf{E}(\tilde{\mathbf{\theta}})].$$

(49)

The covariance matrix of $\mathbf{\underset{\sim}{K}}_m(\tilde{\mathbf{\theta}})$ is calculated as follows:

$$\mathbf{Cov}\left[\mathbf{\underset{\sim}{K}}_m(\tilde{\mathbf{\theta}})\right] = \frac{1}{r-1} \sum_{k=1}^{r} \left\{ \mathbf{\underset{\sim}{K}}_m(\tilde{\mathbf{\theta}}_k) \cdot \mathbf{\underset{\sim}{K}}_m[\mathbf{E}(\tilde{\mathbf{\theta}})] \right\}^T \cdot \left\{ \mathbf{\underset{\sim}{K}}_m(\tilde{\mathbf{\theta}}_k) \cdot \mathbf{\underset{\sim}{K}}_m[\mathbf{E}(\tilde{\mathbf{\theta}})] \right\}$$

$$= \frac{1}{r-1} \sum_{k=1}^{r} \left\{ [\tilde{\mathbf{\theta}}_k - \mathbf{E}(\tilde{\mathbf{\theta}})] \cdot \mathbf{N}_\theta[\mathbf{E}(\tilde{\mathbf{\theta}})] \right\}^T \cdot \left\{ [\tilde{\mathbf{\theta}}_k - \mathbf{E}(\tilde{\mathbf{\theta}})] \cdot \mathbf{N}_\theta[\mathbf{E}(\tilde{\mathbf{\theta}})] \right\}$$

$$= \mathbf{N}_\theta[\mathbf{E}(\tilde{\mathbf{\theta}})]^T \cdot [\mathbf{Cov}(\tilde{\mathbf{\theta}})] \cdot \mathbf{N}_\theta[\mathbf{E}(\tilde{\mathbf{\theta}})].$$

(50)

Based on the calculation method of Eqs. (49) and (50), the mean $\mathbf{E}\left[\mathbf{\underset{\sim}{k}}_{m,w}(\tilde{\mathbf{\theta}})\right]$ and covariance $\mathbf{Cov}\left[\mathbf{\underset{\sim}{k}}_{m,w}(\tilde{\mathbf{\theta}})\right]$ of the stacked vector of the stiffness matrix of any element w is obtained. Using the relationship between the transfer function matrix and the global stiffness matrix shown in Eq. (8), the mean of the transfer function matrix is obtained as follows:

$$\mathbf{E}[\mathbf{G}_m(\tilde{\mathbf{\theta}})] = \{ \mathbf{M}_m s^2 + \mathbf{C}_m s + \mathbf{E}[\mathbf{K}_m(\tilde{\mathbf{\theta}})] \}^{-1}.$$

(51)

The covariance matrix of the stacked vector $\mathbf{\underset{\sim}{G}}_m(\tilde{\mathbf{\theta}})$ of the transfer function matrix is expressed as:

$$\mathbf{Cov}\left[\mathbf{\underset{\sim}{G}}_m(\tilde{\mathbf{\theta}})\right] = \mathbf{N}_K\left[\mathbf{\underset{\sim}{K}}_m(\tilde{\mathbf{\theta}})\right]^T \cdot \left\{ \mathbf{Cov}\left[\mathbf{\underset{\sim}{K}}_m(\tilde{\mathbf{\theta}})\right] \right\} \cdot \mathbf{N}_K\left[\mathbf{\underset{\sim}{K}}_m(\tilde{\mathbf{\theta}})\right],$$

(52)

where $\mathbf{N}_K\left[\mathbf{\underset{\sim}{K}}_m(\tilde{\mathbf{\theta}})\right]$ is the sensitivity matrix of $\mathbf{\underset{\sim}{G}}_m(\tilde{\mathbf{\theta}})$ with respect to $\mathbf{\underset{\sim}{K}}_m(\tilde{\mathbf{\theta}})$, $\mathbf{N}_K\left[\mathbf{\underset{\sim}{K}}_m(\tilde{\mathbf{\theta}})\right] \in \mathbb{R}^{n^2 \times n^2}$. According to the derivative formula of the inverse matrix, the following equation is obtained:

$$\Delta \mathbf{G}_m = -(\mathbf{M}_m s^2 + \mathbf{C}_m s + \mathbf{K}_m)^{-1} \cdot \Delta \mathbf{K}_m \cdot (\mathbf{M}_m s^2 + \mathbf{C}_m s + \mathbf{K}_m)^{-1}.$$

(53)

Then, the expression of $\mathbf{N}_K\left[\mathbf{\underset{\sim}{K}}_m(\tilde{\mathbf{\theta}})\right]$ is obtained as follows:

$$\mathbf{N}_K\left[\mathbf{\underset{\sim}{K}}_m(\tilde{\mathbf{\theta}})\right] = -\left\{ \left[\mathbf{M}_m s^2 + \mathbf{C}_m s + \mathbf{E}(\mathbf{K}_m(\tilde{\mathbf{\theta}}))\right]^{-1} \right\}^T$$

$$\otimes \left[\mathbf{M}_m s^2 + \mathbf{C}_m s + \mathbf{E}(\mathbf{K}_m(\tilde{\mathbf{\theta}}))\right]^{-1},$$

(54)

where $\otimes$ denotes the Kronecker product. According to Eqs. (50), (52) and (54), $\mathbf{Cov}\left[\mathbf{\underset{\sim}{G}}_m(\theta)\right]$ is expressed as:

$$\mathbf{Cov}\Big[\underset{\sim}{\mathbf{G}}_{\mathrm{m}}(\tilde{\boldsymbol{\theta}})\Big] = \left\{ -\Big\{ \big[\mathbf{M}_{\mathrm{m}}s^2 + \mathbf{C}_{\mathrm{m}}s + \mathbf{E}\big(\mathbf{K}_{\mathrm{m}}(\tilde{\boldsymbol{\theta}})\big)\big]^{-1} \Big\}^{\mathrm{T}} \otimes \big[\mathbf{M}_{\mathrm{m}}s^2 + \mathbf{C}_{\mathrm{m}}s + \mathbf{E}\big(\mathbf{K}_{\mathrm{m}}(\tilde{\boldsymbol{\theta}})\big)\big]^{-1} \Big\}^{\mathrm{T}} \right.$$
$$\cdot \Big\{ \mathbf{N}_{\boldsymbol{\theta}}\big[\mathbf{E}(\tilde{\boldsymbol{\theta}})\big]^{\mathrm{T}} \cdot \big[\mathbf{Cov}(\tilde{\boldsymbol{\theta}})\big] \cdot \mathbf{N}_{\boldsymbol{\theta}}\big[\mathbf{E}(\tilde{\boldsymbol{\theta}})\big] \Big\} \cdot \Big\{ -\Big\{ \big[\mathbf{M}_{\mathrm{m}}s^2 + \mathbf{C}_{\mathrm{m}}s + \mathbf{E}\big(\mathbf{K}_{\mathrm{m}}(\tilde{\boldsymbol{\theta}})\big)\big]^{-1} \Big\}^{\mathrm{T}}$$
$$\left. \otimes \big[\mathbf{M}_{\mathrm{m}}s^2 + \mathbf{C}_{\mathrm{m}}s + \mathbf{E}\big(\mathbf{K}_{\mathrm{m}}(\tilde{\boldsymbol{\theta}})\big)\big]^{-1} \right\}. \tag{55}$$

The mean and variance of each element in the transfer function matrix $\mathbf{G}_{\mathrm{m}}(\tilde{\boldsymbol{\theta}})$ and element stiffness matrix $\mathbf{k}_{\mathrm{m},w}(\tilde{\boldsymbol{\theta}})$ are extracted from the calculation results of Eqs. (48)–(52).

Appendix III. Sensitivity calculation method with complex perturbation

The sensitivity calculation method based on complex perturbations only needs numerical calculations to solve the sensitivity problem, which can avoid complicated derivation operations. According to Eq. (47), the definition of $\underset{\sim}{\mathbf{K}}_{\mathrm{m}}(\tilde{\boldsymbol{\theta}}_k)$ is as follows:

$$\underset{\sim}{\mathbf{K}}_{\mathrm{m}}(\tilde{\boldsymbol{\theta}}_k) = \Big[K_{\mathrm{m}}^1(\tilde{\boldsymbol{\theta}}_k), K_{\mathrm{m}}^2(\tilde{\boldsymbol{\theta}}_k), \cdots, K_{\mathrm{m}}^b(\tilde{\boldsymbol{\theta}}_k), \cdots, K_{\mathrm{m}}^{n^2}(\tilde{\boldsymbol{\theta}}_k) \Big]. \tag{56}$$

The mean vector $\mathbf{E}(\tilde{\boldsymbol{\theta}})$ of the updating parameters is added to a small imaginary part, which is denoted by the complex vector $\mathbf{E}(\tilde{\boldsymbol{\theta}}) + \Delta\boldsymbol{\theta}_{v_0}\mathbf{j}$. The Taylor series expansion of the complex function $K_{\mathrm{m}}^b\big[\mathbf{E}(\tilde{\boldsymbol{\theta}}) + \Delta\boldsymbol{\theta}_{v_0}\mathbf{j}\big]$ is defined as:

$$K_{\mathrm{m}}^b\big[\mathbf{E}(\tilde{\boldsymbol{\theta}}) + \Delta\boldsymbol{\theta}_{v_0}\mathbf{j}\big] = K_{\mathrm{m}}^b\big[\mathbf{E}(\tilde{\boldsymbol{\theta}})\big] + \frac{\partial K_{\mathrm{m}}^b\big[\mathbf{E}(\tilde{\boldsymbol{\theta}})\big]}{\partial\mathbf{E}(\tilde{\boldsymbol{\theta}})}\Delta\theta_{v_0}j$$
$$- \frac{\big(\Delta\theta_{v_0}\big)^2}{2!}\frac{\partial^2 K_{\mathrm{m}}^b\big[\mathbf{E}(\tilde{\boldsymbol{\theta}})\big]}{\partial^2\mathbf{E}(\tilde{\boldsymbol{\theta}})} + \frac{\big(\Delta\theta_{v_0}\big)^3}{3!}\frac{\partial^3 K_{\mathrm{m}}^b\big[\mathbf{E}(\tilde{\boldsymbol{\theta}})\big]}{\partial^3\mathbf{E}(\tilde{\boldsymbol{\theta}})} + \cdots, \tag{57}$$

where j represents a complex index; $\mathbf{j}$ represents a set of complex indexes; and $\Delta\boldsymbol{\theta}_{v_0}$ is the complex perturbation added to $\mathbf{E}(\tilde{\boldsymbol{\theta}})$. $\mathbf{E}(\tilde{\boldsymbol{\theta}}) \in \mathbb{R}^{1\times v}$ and $\Delta\boldsymbol{\theta}_{v_0} \in \mathbb{R}^{1\times v}$ are expressed as:

$$\mathbf{E}(\tilde{\boldsymbol{\theta}}) = \big\{ \mathrm{E}(\tilde{\theta}_1), \mathrm{E}(\tilde{\theta}_2), \cdots, \mathrm{E}(\tilde{\theta}_{v_0}), \cdots, \mathrm{E}(\tilde{\theta}_v) \big\}, \tag{58}$$

$$\Delta\boldsymbol{\theta}_{v_0} = \big\{ 0, 0, \cdots, \Delta\theta_{v_0}, \cdots, 0 \big\}. \tag{59}$$

The imaginary part of $K_{\mathrm{m}}^b\big[\mathbf{E}(\tilde{\boldsymbol{\theta}}) + \Delta\boldsymbol{\theta}_{v_0}\mathbf{j}\big]$ is extracted as:

$$J\big\{ K_{\mathrm{m}}^b\big[\mathbf{E}(\tilde{\boldsymbol{\theta}}) + \Delta\boldsymbol{\theta}_{v_0}\mathbf{j}\big] \big\} = \frac{\partial K_{\mathrm{m}}^b\big[\mathbf{E}(\tilde{\boldsymbol{\theta}})\big]}{\partial\mathbf{E}(\tilde{\boldsymbol{\theta}})}\Delta\theta_{v_0} + O\Big[\big(\Delta\theta_{v_0}\big)^3\Big], \tag{60}$$

where $J\{\cdot\}$ denotes the imaginary parts of $K_{\mathrm{m}}^b\big[\mathbf{E}(\tilde{\boldsymbol{\theta}}) + \Delta\boldsymbol{\theta}_{v_0}\mathbf{j}\big]$ and $O(\cdot)$ denotes the higher-order infinitesimal. Then, the sensitivity is obtained by the following equation:

$$\frac{\partial K_{\mathrm{m}}^b\big[\mathbf{E}(\tilde{\boldsymbol{\theta}})\big]}{\partial\mathbf{E}(\tilde{\boldsymbol{\theta}})} = \frac{J\big\{ K_{\mathrm{m}}^b\big[\mathbf{E}(\tilde{\boldsymbol{\theta}}) + \Delta\boldsymbol{\theta}_{v_0}\mathbf{j}\big] \big\}}{\Delta\theta_{v_0}} \tag{61}$$

On this basis, the sensitivity matrix $\mathbf{N}_{\boldsymbol{\theta}}\big[\mathbf{E}(\tilde{\boldsymbol{\theta}})\big]$ of $\underset{\sim}{\mathbf{K}}_{\mathrm{m}}(\tilde{\boldsymbol{\theta}}_k)$ corresponding to $\mathbf{E}(\tilde{\boldsymbol{\theta}})$ is obtained as follows:

$$\mathbf{N}_{\boldsymbol{\theta}}\big[\mathbf{E}(\tilde{\boldsymbol{\theta}})\big] = \left\{ \frac{\partial K_{\mathrm{m}}^1\big[\mathbf{E}(\tilde{\boldsymbol{\theta}})\big]}{\partial\mathbf{E}(\tilde{\boldsymbol{\theta}})}, \frac{\partial K_{\mathrm{m}}^2\big[\mathbf{E}(\tilde{\boldsymbol{\theta}})\big]}{\partial\mathbf{E}(\tilde{\boldsymbol{\theta}})}, \cdots, \frac{\partial K_{\mathrm{m}}^{n^2}\big[\mathbf{E}(\tilde{\boldsymbol{\theta}})\big]}{\partial\mathbf{E}(\tilde{\boldsymbol{\theta}})} \right\}. \tag{62}$$

References

1. Yang MJ, Zhong H, Telste M et al (2016) Bridge damage localization through modified curvature method. J Civ Struct Health Monit 6(1):175–188. https://doi.org/10.1007/s13349-015-0150-7
2. Zhang WW, Li J, Hao H et al (2017) Damage detection in bridge structures under moving loads with phase trajectory change of multi-type vibration measurements. Mech Syst Signal process 87:410–425. https://doi.org/10.1016/j.ymssp.2016.10.035
3. Salane HJ, Baldwin JW (1990) Identification of modal properties of bridges. J Struct Eng 116(7):2008–2021. https://doi.org/10.1061/(ASCE)0733-9445(1990)116:7(2008)
4. Ercolani GD, Felix DH, Ortega NF (2018) Crack detection in prestressed concrete structures by measuring their natural frequencies. J Civ Struct Health Monit 8(4):661–671. https://doi.org/10.1007/s13349-018-0295-2
5. Xia Y, Chen B, Zhou XQ et al (2013) Field monitoring and numerical analysis of Tsing Ma Suspension Bridge temperature behavior. Struct Control Health Monit 20(4):560–575. https://doi.org/10.1002/stc.515
6. Liu Y, Zhang SY (2017) Probabilistic Baseline of finite element model of bridges under environmental temperature changes. Comput Aided Civ Infrastruct Eng 32(7):581–598. https://doi.org/10.1111/mice.12268
7. Obrien EJ, Martinez D, Malekjafarian A et al (2017) Damage detection using curvatures obtained from vehicle measurements. J Civ Struct Health Monit 7(3):333–341. https://doi.org/10.1007/s13349-017-0233-8
8. Moughty JJ, Casas JR (2017) A state of the art review of modal-based damage detection in bridges: development, challenges, and solutions. Appl Sci 7(5):510. https://doi.org/10.3390/app7050510

9. Liu X, Lieven NAJ, Escamilla-Ambrosio PJ (2009) Frequency response function shape based methods for structural damage localization. Mech Syst Signal process 23:1243–1259. https://doi.org/10.1016/j.ymssp.2008.10.002

10. Catbas FN, Brown DL, Aktan AE (2006) Use of modal flexibility for damage detection and condition assessment: case studies and demonstrations on large structures. J Struct Eng 132:1699–1712. https://doi.org/10.1061/(ASCE)0733-9445(2006)132:11(1699)

11. An YH, Blachowski B, Ou JP (2016) A degree of dispersion-based damage localization method. Struct Control Health Monit 23(1):176–192. https://doi.org/10.1002/stc.1760

12. Shahsavari V, Bastien J, Chouinard L et al (2017) Likelihood-based testing of wavelet coefficients for damage detection in beam structures. J Civ Struct Health Monit 7(1):79–98. https://doi.org/10.1007/s13349-017-0212-0

13. Mashayekhi M, Santini-Bell E, Azam SE (2021) Fatigue crack detection in welded structural components of steel bridges using artificial neural network. J Civ Struct Health Monit. https://doi.org/10.1007/s13349-021-00488-7

14. Sharma S, Sen S (2020) One-dimensional convolutional neural network-based damage detection in structural joints. J Civ Struct Health Monit 10(5):1057–1072. https://doi.org/10.1007/s13349-020-00434-z

15. Kim CW, Morita T, Oshima Y et al (2015) A Bayesian approach for vibration-based long-term bridge monitoring to consider environmental and operational changes. Smart Struct Syst 15(2):395–408. https://doi.org/10.12989/sss.2015.15.2.395

16. Bernal D (2002) Load vectors for damage localization. J Eng Mech 128(1):7–14. https://doi.org/10.1061/(ASCE)0733-9399(2002)128:1(7)

17. Bernal D (2006) Flexibility-based damage localization from stochastic realization results. J Eng Mech 132(6):651–658. https://doi.org/10.1061/(ASCE)0733-9399(2006)132:6(651)

18. Bernal D (2007) Damage localization from the null space of changes in the transfer matrix. AIAA J 45(2):374–381. https://doi.org/10.2514/1.25037

19. Bernal D (2010) Load vectors for damage location in systems identified from operational loads. J Eng Mech 136(1):31–39. https://doi.org/10.1061/(ASCE)EM.1943-7889.0000067

20. Gao Y, Spencer BFJ, Bernal D (2007) Experimental verification of the flexibility-based damage locating vector method. J Eng Mech 133(10):1043–1049. https://doi.org/10.1061/(ASCE)0733-9399(2007)133:10(1043)

21. Jang S, Sim SH, Jo H et al (2012) Full-scale experimental validation of decentralized damage identification using wireless smart sensors. Smart Mater Struct 21(11):115019. https://doi.org/10.1088/0964-1726/21/11/115019

22. Jang S, Spencer BFJ, Rice JA et al (2011) Full-Scale Experimental Validation of High-Fidelity Wireless Measurement on a Historic Truss Bridge. Adv Struct Eng 14(1):93–101. https://doi.org/10.1260/1369-4332.14.1.93

23. Maeck J, Peeters B, De Roeck G (2001) Damage identification on the Z24-bridge using vibration monitoring. Smart Mater Struct 10(5):512–517. https://doi.org/10.1088/0964-1726/10/3/313

24. Xia Y, Hao H, Zanardo G (2006) Long term vibration monitoring of an RC slab: temperature and humidity effect. Eng Struct 28:441–452. https://doi.org/10.1016/j.engstruct.2005.09.001

25. Giraldo DF, Dyke SJ, Caicedo JM (2006) Damage detection accommodating varying environmental conditions. Struct Health Monit 5(2):155–172. https://doi.org/10.1177/1475921706057987

26. Peeters B, Roeck GD (2001) One-year monitoring of the Z24-bridge: Environmental effects versus damage events. Earthquake Eng Struct Dyn 30(2):149–171. https://doi.org/10.1002/1096-9845(200102)30:2%3c149::AID-EQE1%3e3.0.CO;2-Z

27. Liu C, DeWolf JT (2007) Effect of temperature on modal variability of a curved concrete bridge under ambient loads. J Struct Eng 133(12):1742–1751. https://doi.org/10.1061/(ASCE)0733-9445(2007)133:12(1742)

28. Farrar CR, Jauregui DA (1998) Comparative study of damage identification algorithms applied to a bridge: I. Exp Smart Mater Struct 7(5):720–731. https://doi.org/10.1088/0964-1726/7/5/013

29. Jang S, Dahal S (2015) Full-Scale Application of Stochastic DLV Method for Highway Bridge Health Monitoring. Adv Struct Eng 18(11):1875–1885. https://doi.org/10.1260/1369-4332.18.11.1875

30. Döhler M, Marin L, Bernal D et al (2013) Statistical decision making for damage localization with stochastic load vectors. Mech Syst Signal Process 39(1–2):426–440. https://doi.org/10.1016/j.ymssp.2012.12.011

31. Marin L, Döhler M, Bernal D et al (2015) Robust statistical damage localization with stochastic load vectors. Struct Control Health Monit 22(3):557–573. https://doi.org/10.1002/stc.1686

32. Bhuyan M, Döhler M, Lecieux Y et al (2017) Statistical damage localization with stochastic load vectors using multiple mode sets. Struct Health Monit 16(5):518–535. https://doi.org/10.1177/1475921717714447

33. Bhuyan M, Gautier G, Touz N et al (2019) Vibration-based damage localization with load vectors under temperature changes. Struct Control Health Monit 26(11):e2439. https://doi.org/10.1002/stc.2439

34. Ko JM, Chak KK, Wang JY et al (2003) Formulation of an uncertainty model relating modal parameters and environmental factors by using long-term monitoring data, In: Proceedings of the SPIE smart structures and materials 2003 conference, San Diego, USA.

35. Kullaa J (2009) Eliminating environmental or operational influences in structural health monitoring using the missing data analysis. J Intel Mat Syst Str 20(11):1381–1390. https://doi.org/10.1177/1045389X08096050

36. Xia Y, Chen B, Weng S et al (2012) Temperature effect on vibration properties of civil structures: a literature review and case studies. J Civ Struct Health Monit 2:29–46

37. Shokrani Y, Dertimanis VK, Chatzi EN et al (2018) On the use of mode shape curvatures for damage localization under varying environmental conditions. Struct Control Health Monit 25(4):e2132. https://doi.org/10.1002/stc.2132

38. Jin CH, Jang SA, Sun XR et al (2016) Damage detection of a highway bridge under severe temperature changes using extended Kalman filter trained neural network. J Civ Struct Health Monit 6(3):545–560. https://doi.org/10.1007/s13349-016-0173-8

39. Yan AM, Kerschen G, De Boe P et al (2005) Structural damage diagnosis under varying environmental conditions-part II: Local PCA for non-linear cases. Mech Syst Signal Process 19(4):865–880. https://doi.org/10.1016/j.ymssp.2004.12.003

40. Zheng W, Qian F, Shen JL et al (2020) Mitigating effects of temperature variations through probabilistic-based machine learning for vibration-based bridge scour detection. J Civ Struct Health Monit 10(5):957–972. https://doi.org/10.1007/s13349-020-00427-y

41. Sohn H, Dzwonczyk M, Straser EG et al (1999) An experimental study of temperature effect on modal parameters of the Alamosa Canyon Bridge. Earthq Eng Struct D 28(8):879–897. https://doi.org/10.1002/(SICI)1096-9845(199908)28:8%3c879::AID-EQE845%3e3.3.CO;2-M

42. Wang GX, Ye JH (2019) Localization and quantification of partial cable damage in the long-span cable-stayed bridge using the abnormal variation of temperature-induced girder deflection. Struct Control Health Monit 26(1):e2281. https://doi.org/10.1002/stc.2281

43. Fallahian M, Khoshnoudian F, Meruane V (2018) Ensemble classification method for structural damage assessment under varying

temperature. Struct Health Monit 7(4):747–762. https://doi.org/10.1177/1475921717717311

44. Wang LX, Li XY, Tan Y et al (2015) Long-term health monitoring of in-service bridge deck by covariance of covariance matrix of acceleration responses. Adv Struct Eng 18(12):2129–2149. https://doi.org/10.1260/1369-4332.18.12.2129

45. Zhang HY, Gül M, Kostić B (2019) Eliminating Temperature Effects in Damage Detection for Civil Infrastructure Using Time Series Analysis and Autoassociative Neural Networks. J Aeros Eng 32(2):04019001. https://doi.org/10.1061/(ASCE)AS.1943-5525.0000987

46. Zhang SY, Liu Y (2020) Damage detection of bridges monitored within one cluster based on the residual between the cumulative distribution functions of strain monitoring data. Struct Health Monit 19(6):1764–1789. https://doi.org/10.1177/1475921719895955

47. Cao JX, Liu Y, Li CP (2021) Damage cross detection between bridges monitored within one cluster using the difference ratio of projected strain monitoring data. Struct Health Monit. https://doi.org/10.1177/14759217211006792

48. Kokkinakis K, Nandi AK (2005) Exponent parameter estimation for generalized Gaussian probability density functions with application to speech modeling. Signal Process 85(9):1852–1858. https://doi.org/10.1016/j.sigpro.2005.02.017

49. Meruane V, Heylen W (2011) Structural damage assessment under varying temperature conditions. Struct Health Monit 11(3):345–357. https://doi.org/10.1177/1475921711419995

50. Wang X, Gao QF, Liu Y (2020) Damage detection of bridges under environmental temperature changes using a hybrid method. Sensors 20(14):3999. https://doi.org/10.3390/s20143999

51. Farrar CR, James GH (1997) System identification from ambient vibration measurements on a bridge. J Sound Vib 205(1):1–18. https://doi.org/10.1006/jsvi.1997.0977.

52. Adeli H, Cheng NT (1993) Integrated genetic algorithm for optimization of space structures. J Aeros Eng 6(4):315–328. https://doi.org/10.1061/(ASCE)0893-1321(1993)6:4(315)

53. Redner RA, Walker HF (1984) Mixture densities, maximum likelihood and the EM algorithm. SIAM Rev 26(2):195–239

54. Bernal D (2012) Sensitivies of eigenvalues and eigenvectors from complex perturbations, in Topics in Modal Analysis II, vol. 6, Springer, New York, pp. 589–593. https://doi.org/10.1007/978-1-4614-2419-2_59